Chemical Engineering Journal 148 (2009) 145–163

Contents lists available at ScienceDirect

Chemical Engineering Journal

journal homepage: www.elsevier.com/locate/cej

Analysis of the bubbling behaviour of 2D gas solid fluidized beds Part II. Comparison between experiments and numerical simulations via Digital Image Analysis Technique

Antonio Busciglio, Giuseppa Vella, Giorgio Micale*, Lucio Rizzuti

Dipartimento di Ingegneria Chimica dei Processi e dei Materiali, Facoltà di Ingegneria - Università degli Studi di Palermo, Viale delle Scienze Ed. 6, Palermo 90128, Italy

ARTICLE INFO

Article history:
Received 31 March 2008
Received in revised form 3 November 2008
Accepted 4 November 2008

Keywords:
Fluidization
Computational fluid dynamics
Digital Image Analysis Technique

ABSTRACT

In the field of gas–solid fluidization, bubbles, and all features regarding them, have a very great importance, as they significantly affect the process performance. Numerous experimental studies on bubbles, and their formation, evolution, and properties, have been performed in the past. These investigations appear particularly difficult, due to the nature of these systems, since the gas phase is distributed in both the bubble and the emulsion phase. Several experimental approaches have been developed to tackle this study. Among these, the Digital Image Analysis Technique purposely developed in Part I of the present work, based on the use of a video camera for monitoring the phenomenon coupled with image analysis has been found viable and effective.

Moreover, the bubbles behaviour and characteristics have been described by means of a variety of mathematical models. In recent years, in particular, computational fluid dynamics (CFD) tools have been found to be very effective in providing a powerful framework through which these models can be implemented and numerically solved.

This paper combines both experimental and computational studies, presenting the comparison, performed by DIAT, between experimental data and relevant CFD simulations. In particular, simulations have been performed by means of the ANSYS-CFX code. The comparison comprises the following quantities: bed expansion, bubble hold-up, size evolution, distribution, density, aspect ratio, and bubble velocimetry data.

1. Introduction

Particles and processes involving particles are of paramount importance in the chemical and allied industries. Fluidized beds are widely employed in industrial operations, ranging from the pharmaceutical and food industry, to processes such as catalytic cracking of petroleum, combustion and biomass gasification. The success of fluidized bed processes is due to the fact of their excellent heat and mass transfer characteristics.

Although rather simple in its conception, the application of a fluidized bed process still faces some challenges. First, the performance of the process is strongly influenced by the operative conditions. Secondly, a sound understanding of the mechanisms governing the complex flow phenomena involved in a fluidized bed still remains an open technical and scientific issue.

Many of the characteristic features of gas-fluidized beds, like the excellent solid mixing, heat and mass transfer properties, can be related to the presence of bubbles and are dominated by their behaviour. A deeper knowledge of the fluidized bed hydrodynamics and on how such hydrodynamics are affected by the operative conditions, especially geometry changes and plant scale-up, would provide the base for the development of a fully predictive model.

The gas bubbles rising up through a typical fluidized bed ensure that the particles are circulated throughout the bed so that properties and process conditions could be considered uniform. They have a considerable importance in the fluidized solid–gas systems because they govern hydrodynamics and efficiency of the operation for which the bed is used.

However, the gas contained within the bubbles does not satisfy its prime purpose of interacting with the materials in the bed. As a matter of fact the gas flow in excess of that required to maintain the dense phase at minimum fluidization conditions, flows through the bed in the forms of bubbles and through flow [1]. The fluidization quality of a bed is highly dependent on the distribution of bubbles and their physical properties in the bed such as position, dimen-

* Corresponding author. Tel.: +39 0916567310; fax: +39 0916567280.
E-mail address: micale@dicpm.unipa.it (G. Micale).

1385-8947/$ – see front matter © 2008 Elsevier B.V. All rights reserved.
doi:10.1016/j.cej.2008.11.010

Nomenclature

C_{ds}	drag coefficient, dimensionless
d_p	particle diameter (m)
D_i	strain tensor (s^{-1})
e_s	restitution coefficient
F_g	gas solid momentum exchange coefficient ($kg\,m^{-3}\,s^{-1}$)
g	acceleration due to gravity ($m\,s^{-2}$)
g_0	radial distribution coefficient
I	identity matrix
I_i	interphase momentum exchange ($kg\,m^{-2}\,s^{-2}$)
J_s	source term for granular energy ($kg\,s^{-3}\,m^{-1}$)
k_s	diffusion coefficient for granular energy ($kg\,s^{-1}\,m^{-1}$)
P	pressure (Pa)
Re_s	particle Reynolds number
S_i	stress tensor (Pa)
u	superficial gas velocity ($cm\,s^{-1}$)
u_b	bubble rise velocity ($cm\,s^{-1}$)
v_i	local velocity ($m\,s^{-1}$)

Greek letters

γ_s	collision dissipation energy ($kg\,s^{-3}\,m^{-1}$)
ε_i	volume fraction
λ_i	bulk viscosity ($kg\,s^{-1}\,m^{-1}$)
Θ_s	granular temperature ($m^2\,s^{-2}$)
μ_i	shear viscosity ($kg\,s^{-1}\,m^{-1}$)
ρ_i	density ($kg\,m^{-3}$)
σ_i	effective stress tensor (Pa)
τ_i	tangential stress tensor (Pa)
ϕ	velocity coefficient

Subscripts

g	gas phase
max	maximum
mf	minimum fluidization
s	solid phase
visc.	viscous flow regime

sions, rise and lateral velocity. Ideally, for there to be good quality fluidization the population of bubbles in the bed should be large but the bubbles should be small in size, homogeneously occupy the bed and have low rise velocities. On these grounds clearly appears that studies on bubbles are of primary importance for investigating fluidized beds fluid-dynamics. It is also evident that the principal difficulty in analysing fluidization quality and bubble dynamic is concerned with the possibility of measuring or predicting the physical and geometrical properties of gas bubbles rising in a solid granular medium.

The formation and development of bubbles in the fluid-bed has been extensively studied over a considerable span of time, with the aid of different visualization techniques [2–12].

The widespread application of gas particle flow systems and fluidization in industry demands an increase in efficiency and the development of fundamentally based and realistic mathematical models, accurate and detailed experimental data and design tools for such systems.

The recent development of mathematical modelling of particulate solids behaviour together with the increased computing power enables researchers to simulate the behaviour of fluidized powders and to link fundamental particle properties directly to the powder behaviour and predict the interaction between particles and gaseous or liquid fluids. In this regard, computational fluid dynamics (CFD) modelling provides a fundamental tool to support engineering design and research in multiphase systems. Many authors recognise that computational modelling in multiphase systems has the potential to increase process efficiency and reduce the number of scale-up steps in the design of reliable commercial plants.

In the field of multiphase chemical reaction engineering, CFD modelling has been applied to gas–liquid flows (such as bubble columns) and fluid–solid flows (such as solid–liquid suspensions in stirred tanks, gas–solid fluidized beds).

It is invariably emphasized that a necessary step towards the development of reliable fully predictive CFD models is an extensive experimental validation of the simulation results. It is also worth noting that in the first instance, the experimental validation will come to assess the CFD model chosen to simulate the investigated regimes.

On the above basis, the present work focuses on the simulation of a 2D fluidized bed operating under bubbling and slugging conditions carried out with the use of the commercial CFD code Ansys CFX-10.0. Computational results are post-processed by the Digital Image Analysis Technique presented in Part I [13] of the present work, and eventually compared with experimental data, for assessing their validity.

2. Literature review

The fundamental problem encountered in modelling hydrodynamics of gas–solid fluidized beds is the motion of the involved phases whose interfaces are unstable, with their mutual interactions being understood only for a limited range of conditions [14]. The two-phase system may be described following the classical Eulerian approach of continuum mechanics with boundary and jump conditions to solve the governing equations at the interfaces.

The Eulerian–Eulerian model is the preferred choice for simulating macroscopic hydrodynamics [15]. The general idea in formulating the multi-fluid model is to treat each phase as an interpenetrating continuum, and therefore to construct integral balances of continuity, momentum and energy for both phases, with appropriate boundary conditions and jump conditions for phase interfaces. Since the resultant continuum approximation for the solid phase has no equation of state and lacks variables such as viscosity and normal stress [15], certain averaging techniques and assumptions are required to obtain a complete momentum balance for the solid phase, since transport coefficients of the solid phase must account for gas–particle interactions and particle–particle collisions. In the last decades many investigators tried to develop a theory of particle collision based on the kinetic theory approach by Chapman and Cowling [16]. Numerous studies have shown the capability of the kinetic theory approach for modelling bubbling fluidized beds [15,17–21]. The use of 2D simulations have been extensively adopted because of the ease in obtaining experimental data with respect to full 3D experiments.

Correct prediction of spontaneous bubble formation in freely bubbling gas–solid fluidized beds using Eulerian models, strongly depends on the description of the internal momentum transfer in the particulate phase. This is described in the work by Patil et al. [22], where a simple model, i.e. the Constant Viscosity Model (CVM) is compared with the more complex model based on the Kinetic Theory of Granular Flow (KTGF). CVM describes the solid phase pressure only as a function of a solid porosity by an empirical correlation, assuming the solid phase viscosity to be constant, conversely KTGF describes the solid phase properties in much more detail in terms of instantaneous binary particle–particle interactions. The performance of the KTGF and the CVM in predicting the hydrody-

namics of freely bubbling fluidized beds has been compared with experimental data and correlations taken from the literature.

Once developed appropriate models for the explicit formulation of the solid phase stress tensor, the inter-phase momentum transfer between gas and solid phases is still needed to mathematically close the problem. The momentum exchange (represented by a drag force) is one of the dominant forces in the gas- and solid-phase momentum balances. The drag force on a single sphere in a fluid has been well studied and empirically correlated by Clift et al. [23], and Bird et al. [24], for a wide range of particle Reynolds numbers. However, when a single particle moves in a dispersed two-phase mixture, the drag is affected by the presence of other particles. Numerous correlations for calculating the momentum exchange coefficient of gas–solid systems have been reported in the literatures [25–29].

Despite the modelling challenges, application of CFD to model fluidized bed hydrodynamics continues to develop, as it has many advantages including design optimisation and scale-up of such systems. Some of the correlations used in the models, however, remain to be empirical or semi-empirical. As a result, the model and its parameters must be validated against experimental measurements obtained at similar scale and configurations. Some of the challenges with respect to CFD model validation for gas–solid systems have been reviewed by Grace and Taghipour [30].Gidaspow and Ettehadieh [31], reported a numerical study on the bubble injected in fluidized bed. They calculated the growth, propagation and collapse of bubbles. A comparison between time-averaged void fractions and void fraction measured with a γ-ray densitometry showed that the computer model was able to reproduce correctly the experiment. Due to the limited computational power

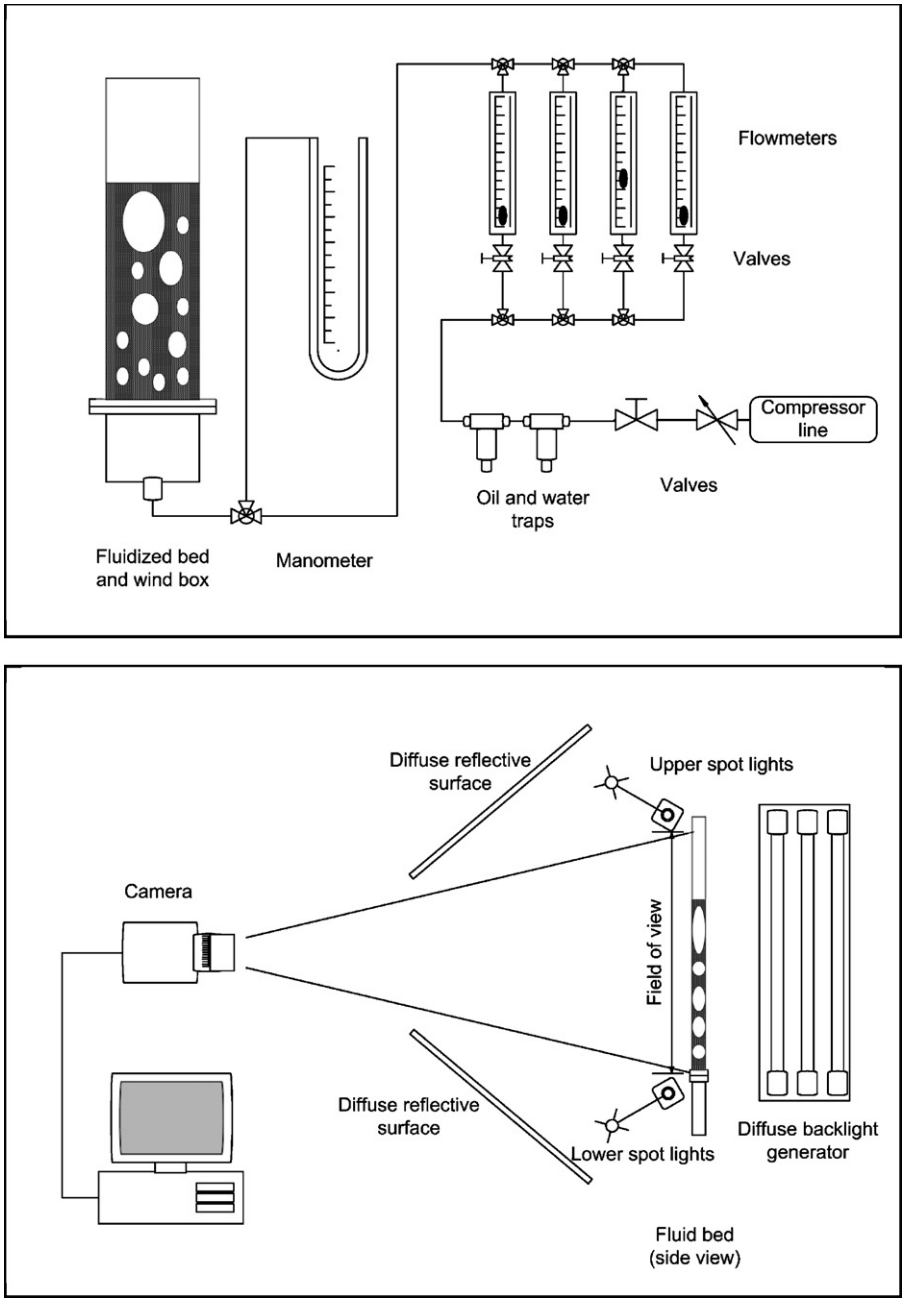

Fig. 1. Experimental set-up: hydraulic (top) and optical (bottom) schemes.

Table 1
Summary of experiments and relevant simulations.

	Case			
	a	b	c	d
u_{mf} (cm s^{-1})	5.24	5.24	5.24	5.24
u (cm s^{-1})	9.0	18.0	27.0	36.0
u/u_{mf}	1.7	3.4	5.0	7.0

available at the time, the analysis was limited to about few seconds and more stringently the two-dimensional simulation was limited to half the bed supposing an axial symmetry of the flow, which has not been confirmed by the experiments.Bouillard et al. [32], simulated a two-dimensional bubbling fluidized bed with an immersed obstacle. Bubble frequencies and sizes were compared to experimental measurements in a thin fluidized bed. Two different hydrodynamic models were compared where the solids stress tensor was modelled by a different formulation of the elasticity modulus. They found good agreement with both models and time-average voidage experimental data, although the models were not able to correctly reproduce the flow field around the obstacle.Ding and Gidaspow [18], simulated a 2D bubbling fluidized bed of a Geldart group B material with a gas jet at the inlet. They used the Jackson governing equations and the granular kinetic model for representing the solids stress tensor. They validated the 2D simulation results by comparing the time-averaged voidage resulting from the simulations with the ones measured experimentally on a two-dimensional fluidized bed, although no further estimate of bubble size was conducted.Kuipers et al. [33], devised a computational model based on the granular kinetic model to simulate the behaviour of a single bubble in a 2D gas fluidized bed with a central orifice. Simulated bubble sizes were compared with experimentally measured data and with predictions obtained by the two-phase theory. Their preliminary calculations showed that the sensitivity of computed bubble size with respect to the bed rheology (i.e. the solid phase viscosity) is quite small, although the bubble shape appeared to be much more sensitive to the bed rheology.

In their paper, Van Wachem et al. [34], validated Eulerian–Eulerian gas–solid model simulations of bubbling fluidized beds with correlations for bubble size and bubble rise velocity available in the literature. Based on 2D simulation results, they compared the bubble sizes obtained from simulations of a freely bubbling gas fluidized bed of a Geldart group B powder with predictions given by Darton et al. [35] correlation. Their results showed that simulated bubble diameters were slightly smaller in the higher part of the fluidized bed, which was attributed to the deficiency of the technique used by Darton to capture small bubbles diameters.

A study of bubbling and slugging fluidized beds using the Eulerian–Eulerian model and the granular kinetic model was proposed by Pain et al. [15]. They simulated a two-dimensional slugging bed of a Geldart group D material using both Cartesian and axi-symmetrical coordinates. The imposed axial symmetry leaded to unphysical results. Some sensitivity of the numerical results to wall friction coefficient was found, while the simulations were relatively insensitive to the coefficient of restitution. An investigation on the effect of a submerged circular obstacle was also carried out. The authors suggested that profiles of the granular temperature can be used to detect areas susceptible of erosion.

In Gelderbloom et al. [21], a multiphase CFD model was applied to a commonly used industrial experiment known as the collapsing fluidized-bed experiment. The experiment involves several hydrodynamic regimes including the bed expansion, bubbling, sedimentation, and consolidation of the fluidized bed. The CFD model is capable of predicting all four of these regimes. Results show that the use of the modified Ergun equation or the MFIX code drag models, and solids rheology have limited impact on the bubbling and collapsing bed simulations. It is also demonstrated that the traditional interpretation of the collapsing bed as consisting of separate bubble escape and sedimentation regimes is incorrect and that, in fact, they occur simultaneously.Peirano et al. [36], proposed a comparison of two- and three-dimensional simulations of turbulent gas–solid flows applied to a stationary bubbling fluidized bed. Based on the Eulerian–Eulerian model formulated by Ishii [37], they employed both the granular kinetic model and the k–ε model for the fluctuating tensors of the solid and particle phases. The numerical results are compared to local instantaneous pressure measurements and time-averaged measurements such as bed height. It was found that significant differences were observed between 2D and 3D simulations. Only 3D simulations can predict the fluid bed hydrodynamics correctly. In addition, they found that the bed height depends on the estimate of the mean particle diameter and that the issue of an accurate prediction of the drag force does not seem to be critical since enough accurate correlations are available.

Two closure models for the internal momentum transfer in the particulate phase have been tested by Patil et al. [38], one semi-empirical model assuming a constant viscosity of the solid phase (CVM) and a second model based on the kinetic theory of granular flow (KTGF), have been compared to describe bubble formation at a single orifice and the time-averaged porosity profiles in the bed using experimental data obtained for a pseudo two-dimensional fluidized bed operated with a jet in the centre.

Correct prediction of spontaneous bubble formation in freely bubbling gas–solid fluidized beds using Eulerian models, strongly depends on the description of the internal momentum transfer in the particulate phase. In Patil et al. [22], the comparison of the simple classical model, describing the solid phase pressure only as a function of a solid porosity by an empirical correlation and assuming the solid phase viscosity constant, which is referred to as the constant viscosity model (CVM), with the more fundamental model based on the kinetic theory of granular flow (KTGF), in which the solid phase properties are described in much more detail in terms of instantaneous binary particle–particle interactions, has been extended for freely bubbling fluidized beds. The performance of the KTGF and the CVM in predicting the hydrodynamics of freely

Table 2
Computational details for preliminary investigation.

	Case				
	Reference case	A	B	C	D
Type	2D	2D	2D	2D	3D
Square cell dimension	5 mm	5 mm	2.5 mm	2.5 mm	2.5 mm
Cells number	288 × 36	288 × 36	576 × 72	576 × 72	576 × 72 × 6
Time step	10^{-3}	10^{-4}	10^{-3}	10^{-4}	10^{-4}
CPU time (h) required for 1 s of real time simulated	3	30	12	120	500

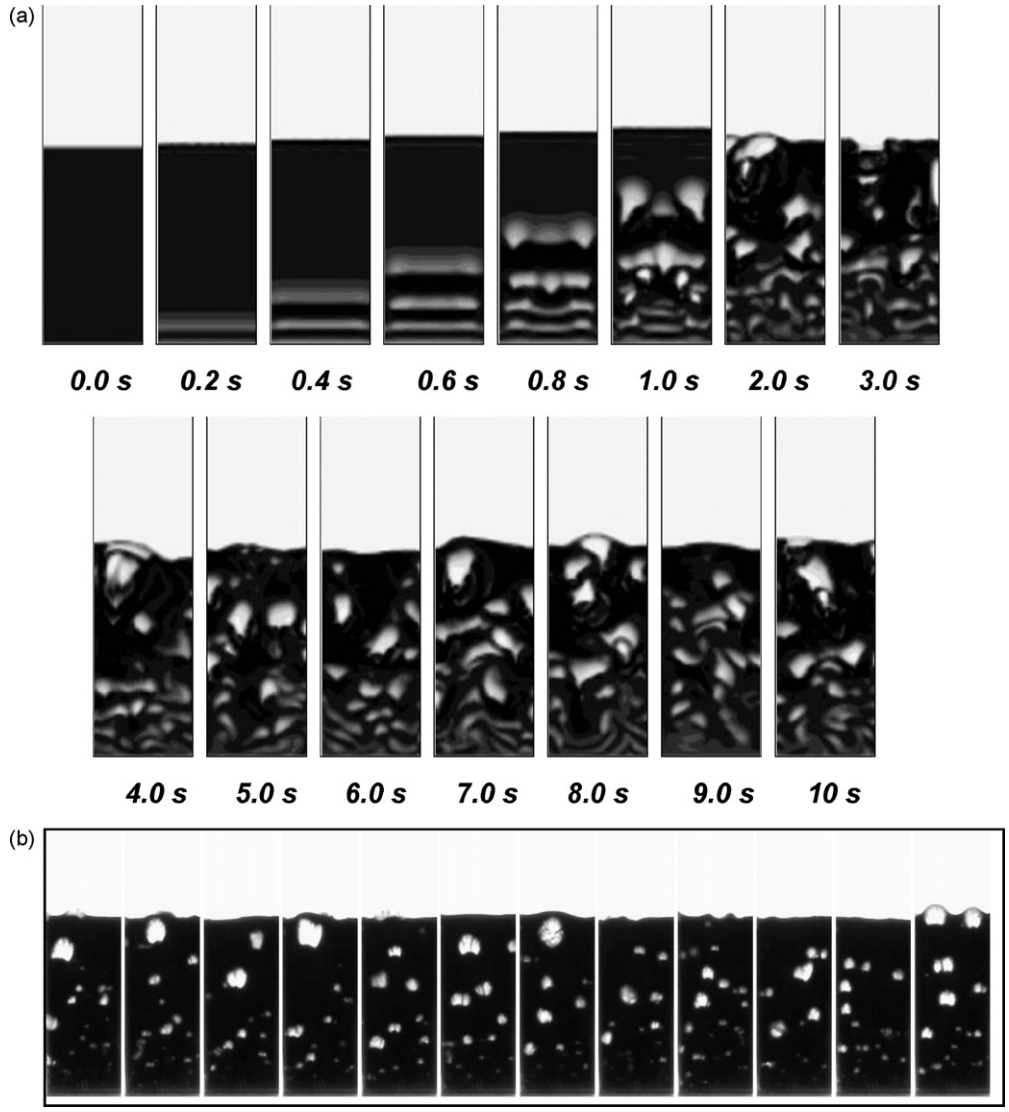

Fig. 2. (a) Simulated maps of volume fraction distributions. Case at $u = 1.7\,u_{mf}$. Stationary bubbling conditions reached after about 2.0 s. (b) Experimental snapshots of the stationary bubbling fluidized bed at $u = 1.7\,u_{mf}$.

bubbling fluidized beds has been compared with experimental data and correlations taken from the literature.

All these previous works reported results of simulations obtained by Eulerian–Eulerian models coupled with the granular kinetic theory. Recently other works have been published on simulation results obtained by the Eulerian–Eulerian Particle Bed Model (PBM [39,40]) and others models developed on the theoretical basis of the PBM [41–45].

The literature review presented above describes a clear evolution in numerical simulations of dense fluidized beds. First, the simulations of dense gas–solid fluidized beds are necessarily time-dependent since the flow phenomena involved present a chaotic nature, which prevent the possibility to reach a steady state. Secondly, the initial simplification of flow symmetries even in presence of geometrical symmetry in non-homogeneous fluidization has not been verified in the validation of the computational results. This has required a greater computational effort to simulate even simple two-dimensional geometries. The availability of increasing computational resources has allowed to simulate a whole bed vessel initially in a two-dimensional form and more recently in a full three-dimensional domain.

Though, two main aspects of the CFD modelling of dense gas-fluidized beds still needs to be addressed. An appropriate choice of the closure relations, which uniquely identifies the Eulerian–Eulerian CFD model, still remains a challenge. Secondly, an extensive validation of 2D simulations results with experimental data needs to be completed both for the characterization of the investigated fluidization regime and for the transition between regimes.

3. Experimental set-up

The fluid-bed reactor purposely designed and built for the present investigation is made of Perspex® with dimensions equal to 800 (height) × 180 (width) × 15 (depth) mm. The whole experimental setup is shown in Fig. 1 (hydraulic scheme).

The reactor is therefore almost two-dimensional, thus allowing visual observations of bubble dynamics within the bed. Glass thin surfaces were inserted to protect front and rear Perspex® walls to avoid surface opacity due to particles attrition phenomena. A plastic porous distributor, whose thickness is equal to 10 mm, is placed at the bottom of the particle bed, and a wind box below the distributor allows to equalize the gas flow.

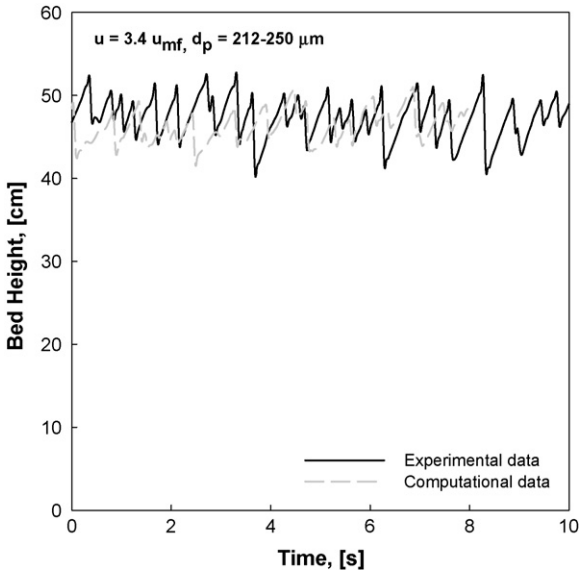

Fig. 3. Comparison between experimental and computational data on instantaneous bed height ($u = 3.4\,u_{mf}$).

Air was used as fluidizing gas, whose flow rate was accurately measured through a set of four flowmeters, covering the range 0–140 l/min. A dehumidifier and an oil filter were also mounted on-line on the gas feed.

Only glass ballotini of size range 212–250 μm were used for the experimental runs with density equal to 2500 kg m^{-3}. The particles were filled up to a bed height of 360 mm, i.e. twice the bed width. The value of u_{mf} was experimentally determined and found equal to 5.24 cm s^{-1}, in agreement with the relevant values obtained by Ergun's correlation. Also the value of gas voidage was experimentally determined and found equal to 0.385. In these conditions the fluidized bed had a typical Geldart Group B system behaviour. The summary of experimental conditions adopted (and relevant simulations) are reported in Table 1.

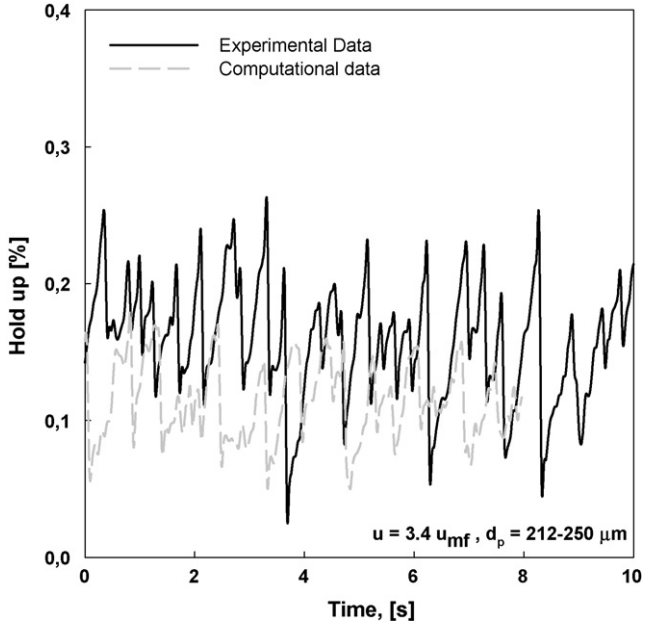

Fig. 5. Comparison between experimental and computational data on instantaneous bubble hold-up ($u = 3.4\,u_{mf}$).

The bubble-related flow structures were visualized with the aid of a back-lighting device and recorded by a commercial digital camcorder (Sony, model DCRTRV530E PAL), placed opposite to the bed at a distance of 270 cm, as shown in Fig. 1 (optical scheme). Continuous high intensity uniform illumination was obtained by placing a diffuse light generator at the backside of the bed, at approximately 10 cm. The digital visual acquisition system allowed to collect images of the bed at a frequency of 25 Hz. Each experimental acquisition provides at least 500 frames, equal to 20 s of real time experiment. The presence of a flange that supports the gas distributor, avoided visual observation of the lowest 0.8 cm of the bed. Preliminarily, the measurement device was accurately cal-

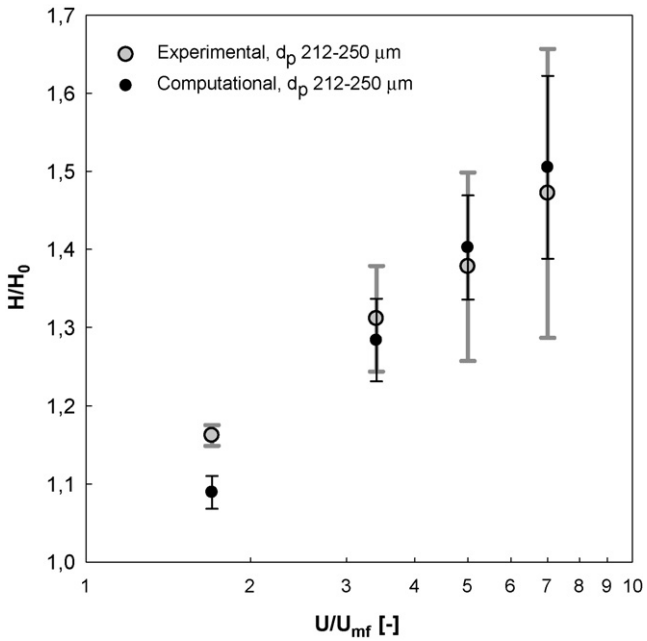

Fig. 4. Comparison of experimental and computational values of mean bed expansion as function of u/u_{mf} ratio.

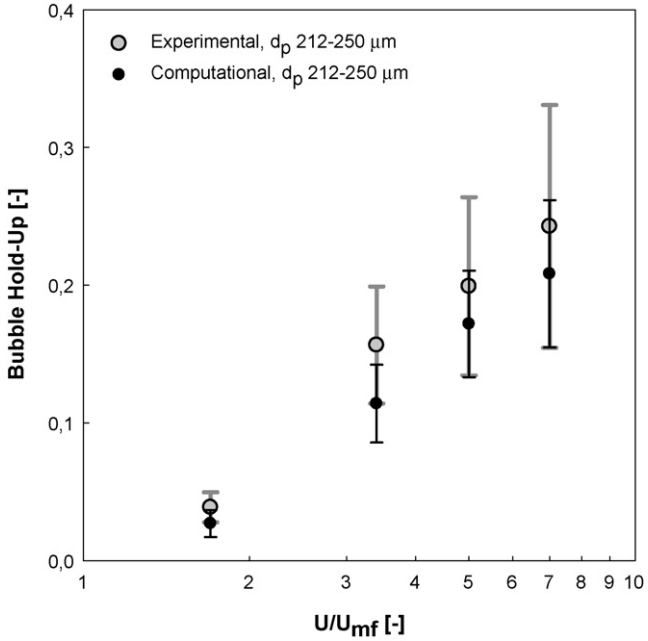

Fig. 6. Comparison of experimental and computational values of mean bubble hold-up as function of u/u_{mf} ratio.

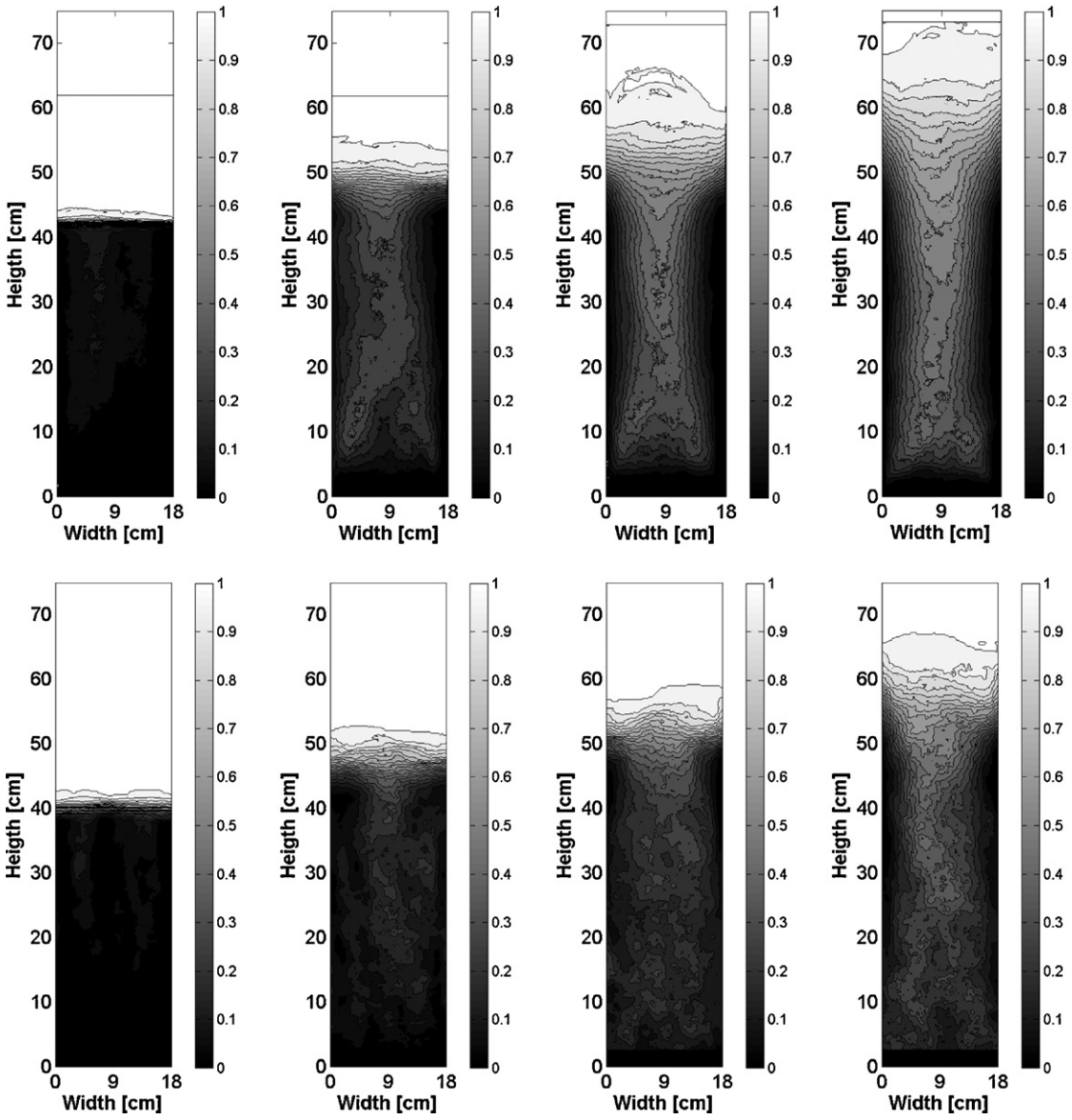

Fig. 7. Comparison between experimental (upper row) and computational (lower row) of time-averaged bubble local hold-up maps at different fluidization velocities. From left to right 1.7 u_{mf}, 3.4 u_{mf}, 5.0 u_{mf} and 7.0 u_{mf}.

ibrated by means of a purposely generated set of still images that included horizontal and vertical scales, with rectangular, circular and ellipsoid objects. The image processing routine was developed on Matlab 7.0 (The MathWorks Inc.), using the Image Processing Toolbox. Thanks to the flexibility of the Matlab environment almost all steps in image processing, data acquiring and elaboration could be easily automated. The reader is referred to Part I of the present work [13] for full details on the experimental set-up adopted and measurement techniques.

4. Computational models and methods

In this study, the Eulerian–Eulerian Multi-phase Flow Model (MFM) coupled with the Granular Kinetic Theory (GKT) has been adopted to study the behaviour of gas–solid fluidized beds. This choice is a standard option of the presently adopted CFD code Ansys CFX-10.

For the present case of two-phase flow, the model has to solve essentially nine equations (one scalar continuity balance equation and three scalar momentum balance equations for each phase involved, plus a volumetric fractions balance equation) in as many unknowns: the two volumetric fractions, the six velocity components and the pressure P (equal for both phases).

Volume fractions balance

$$\varepsilon_g + \varepsilon_s = 1 \tag{1}$$

Mass conservation equation of gas and solid phases

$$\frac{\partial}{\partial t}(\varepsilon_g \rho_g) + \nabla \cdot (\varepsilon_g \rho_g \vec{v_g}) = 0 \tag{2}$$

$$\frac{\partial}{\partial t}(\varepsilon_s \rho_s) + \nabla \cdot (\varepsilon_s \rho_s \vec{v_s}) = 0 \tag{3}$$

Momentum conservation equation of gas and solid phases

$$\frac{\partial}{\partial t}(\varepsilon_g \rho_g \vec{v_g}) + \nabla \cdot (\varepsilon_g \rho_g \vec{v_g} \vec{v_g}) = \nabla \cdot \overline{\overline{S_g}} + \varepsilon_g \rho_g \vec{g} - \vec{I_g} \tag{4}$$

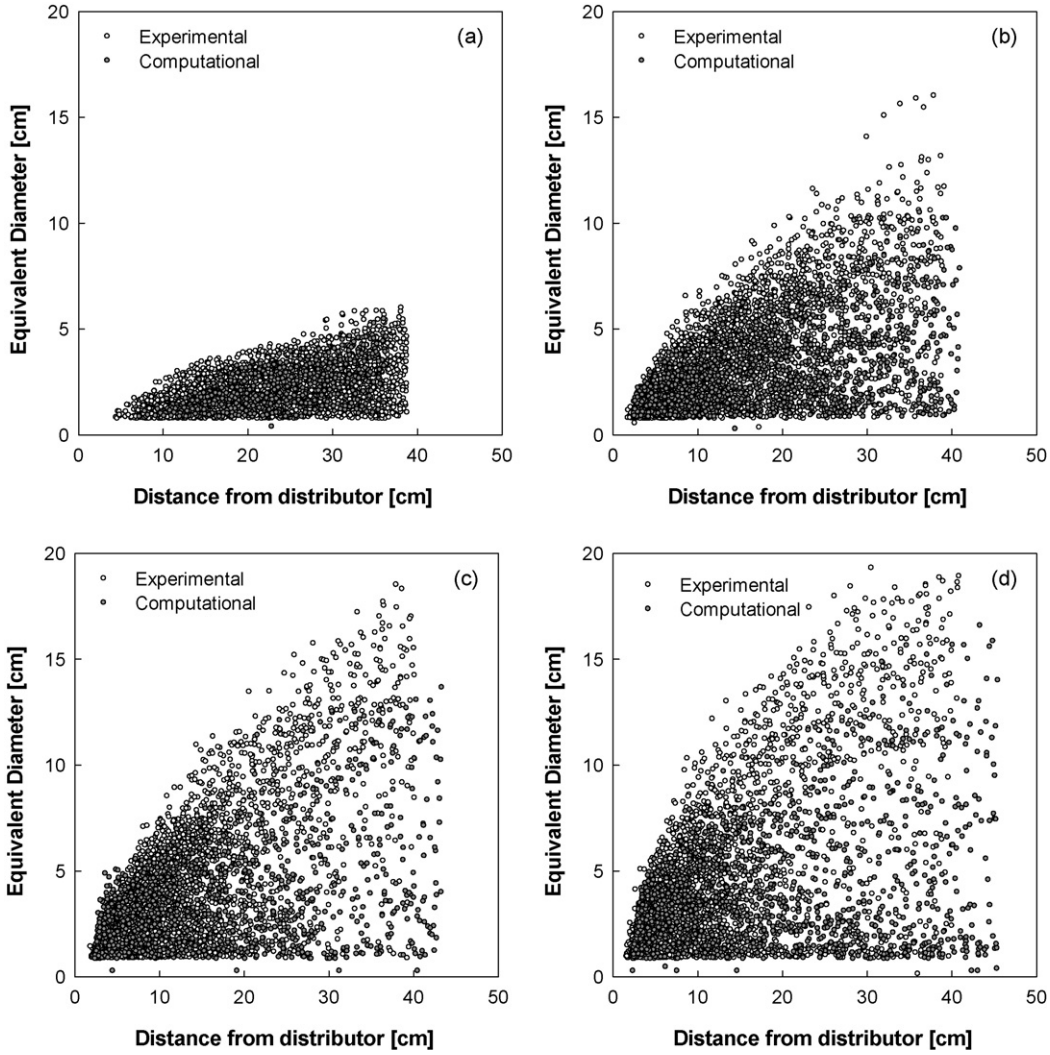

Fig. 8. Comparison of experimental (empty mark) and computational (filled marks) distribution of bubble diameter as function of bubble distance from distributor. (a) 1.7 u_{mf}, (b) 3.4 u_{mf}, (c) 5.0 u_{mf} and (d) 7.0 u_{mf}.

$$\frac{\partial}{\partial t}(\varepsilon_s \rho_s \vec{v_s}) + \nabla \cdot (\varepsilon_s \rho_s \vec{v_s} \vec{v_s}) = \nabla \cdot \overline{\overline{S_s}} + \varepsilon_s \rho_s \vec{g} + \vec{I_g} \quad (5)$$

Continuity and momentum balance equations are thus solved for each phase using a classical Eulerian–Eulerian description. Of course closure relations are also needed in order to properly model the particle phase and its interactions with the gas phase: for this purpose, the standard GKT model is adopted for estimating rheological properties of fluidized solid phase and standard drag models are adopted for estimate the momentum exchange between phases at the phase boundaries. Because of the similarities between particle–particle interactions and molecular interactions in a gas, the concepts from gas kinetic theory can be used to develop a model for the solids stress tensor. Complete details on the derivations and applications to dense phase flow can be found in the work by Gidaspow [28]. The particulate phase is modelled as a population of identical, smooth and inelastic spheres. Particle–particle interactions are described as binary instantaneous collisions, resembling those between gas molecules.

A summary of the relevant closure equations implemented in Ansys CFX 10.0 and selected for the purpose of the present work are reported below.

4.1. Constitutive equations and closure relations

Solid–fluid interphase momentum exchange

$$I_g = -\varepsilon_s \nabla P_g - F_g(\vec{v_s} - \vec{v_g}) \quad (6)$$

Gidaspow drag function

$$F_g = \begin{cases} \frac{3}{4}\frac{\varepsilon_s \varepsilon_g \rho_g}{d_p} C_{ds} \left|\vec{v_s} - \vec{v_g}\right| \varepsilon_s^{-2.65} \Leftrightarrow \varepsilon_g > 0.8 \\ 150\frac{\varepsilon_s^2 \mu_g}{\varepsilon_g d_p^2} + \frac{\varepsilon_s \rho_g}{d_p}\left|\vec{v_s} - \vec{v_g}\right| \Leftrightarrow \varepsilon_g \le 0.8 \end{cases} \quad (7)$$

$$C_{ds} = \frac{24}{\varepsilon_g Re_s}[1 + 0.5(\varepsilon_g Re_s)^{0.687}] \quad (8)$$

$$Re_s = \frac{\rho_g d_p \left|\vec{v_s} - \vec{v_g}\right|}{\mu_g} \quad (9)$$

Fluid phase stress tensor formulation

$$\overline{\overline{S_g}} = -P_g \bar{\bar{I}} + \overline{\overline{\tau_g}} \quad (10)$$

$$\overline{\overline{\tau_g}} = 2\varepsilon_g \mu_g \overline{\overline{D_g}} + \varepsilon_g \lambda_g tr\left(\overline{\overline{D_g}}\right)\bar{\bar{I}} \quad (11)$$

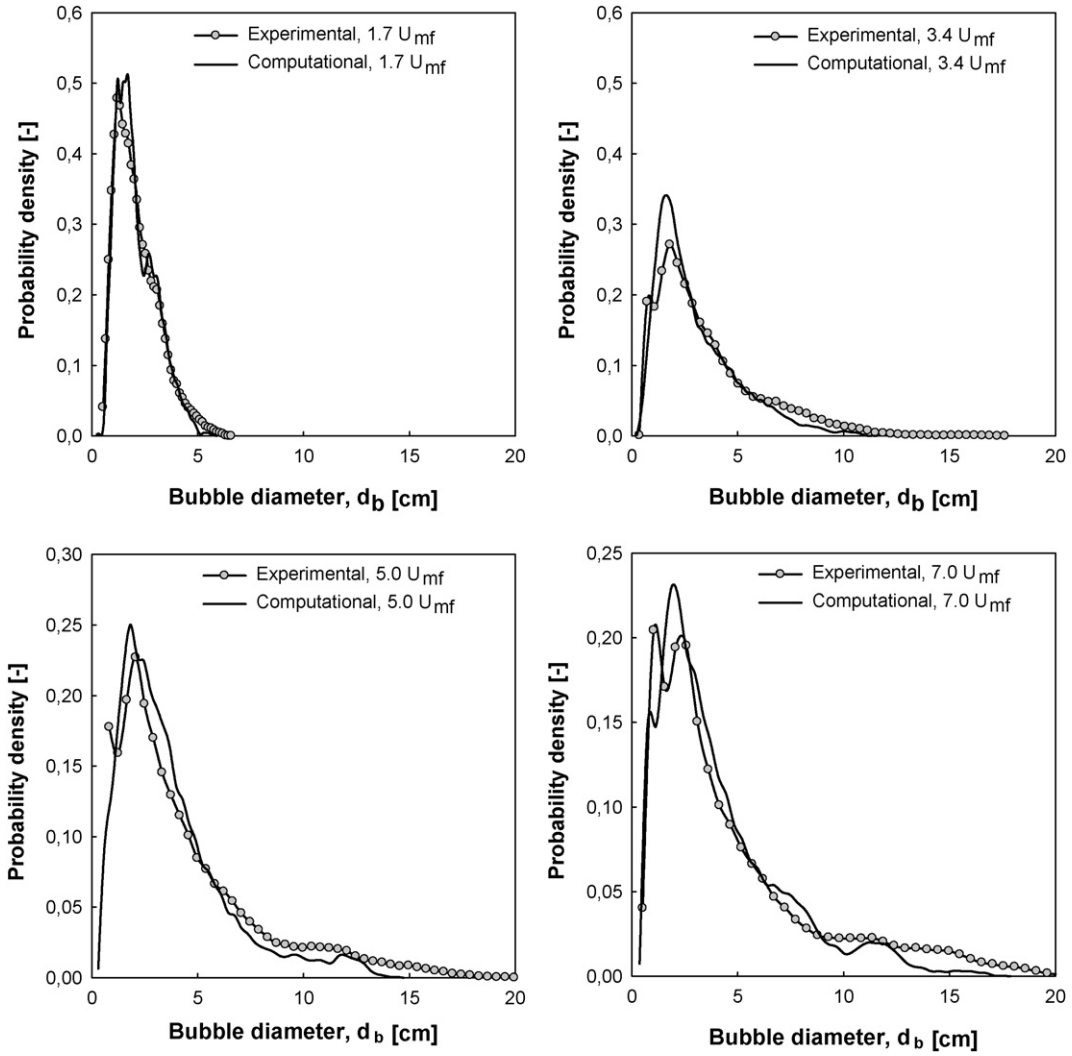

Fig. 9. Comparison of experimental (marks) and computational (lines) probability density distribution of bubble diameter. (a) 1.7 u_{mf}, (b) 3.4 u_{mf}, (c) 5.0 u_{mf} and (d) 7.0 u_{mf}.

$$\overline{\overline{D_g}} = \frac{1}{2}[\nabla \vec{v_g} + (\nabla \vec{v_g})^T] \tag{12}$$

Solids phase stress tensor formulation

$$\overline{\overline{S_s}} = P_s^{visc.}\bar{\bar{I}} - \overline{\overline{\tau_s^{visc.}}} \tag{13}$$

Radial distribution function

$$g_0 = \left[1 - \left(\frac{\varepsilon_s}{\varepsilon_s^{max}}\right)^{1/3}\right]^{-2.5\varepsilon_s^{max}} \tag{14}$$

Collision dissipation energy

$$\gamma_s = \frac{12(1-e_s^2)\rho_s g_0}{d_p\sqrt{\pi}}\varepsilon_s^2\Theta_s^{3/2} \tag{15}$$

Solids pressure equation

$$P_s^{visc.} = \varepsilon_s\rho_s\Theta_s(1 + 2g_0\varepsilon_s(1+e_s)) \tag{16}$$

Solids phase tangential stress equations

$$\overline{\overline{\tau_s^{visc.}}} = 2\mu_s^{visc.}\overline{\overline{D_s}} + \lambda_s^{visc.}tr(\overline{\overline{D_s}})\bar{\bar{I}} \tag{17}$$

$$\overline{\overline{D_s}} = \frac{1}{2}[\nabla \vec{v_s} + (\nabla \vec{v_s})^T] \tag{18}$$

Solids phase bulk viscosity equation

$$\lambda_s = \frac{4}{3}\varepsilon_s\rho_s d_p g_0(1+e_s)\left(\frac{\Theta_s}{\pi}\right)^{0.5} \tag{19}$$

Solids phase shear viscosity equation

$$\mu_s = \frac{4}{5}\varepsilon_s\rho_s d_p g_0(1+e_s)\left(\frac{\Theta_s}{\pi}\right)^{0.5} + \frac{10\rho_s d_p\sqrt{\Theta_s\pi}}{96(1+e_s)\varepsilon_s g_0}\left[1 + \frac{4}{5}g_0\varepsilon_s(1+e_s)\right]^2 \tag{20}$$

4.2. Fluctuation energy conservation equation of solid particles

$$\frac{3}{2}\left[\frac{\partial}{\partial t}(\varepsilon_s\rho_s\Theta_s) + \frac{\partial}{\partial x_i}\cdot(\varepsilon_s\rho_s\Theta_s v_{si})\right] = \sigma_{si,j}\frac{\partial v_{si}}{\partial x_j} - \frac{\partial}{\partial x_i}\cdot\left(k_s\frac{\partial\Theta_s}{\partial x_i}\right) - \gamma_s + J_s \tag{21}$$

The above equation is the complete form of the fluctuation energy conservation equation for the granular phase, which in this

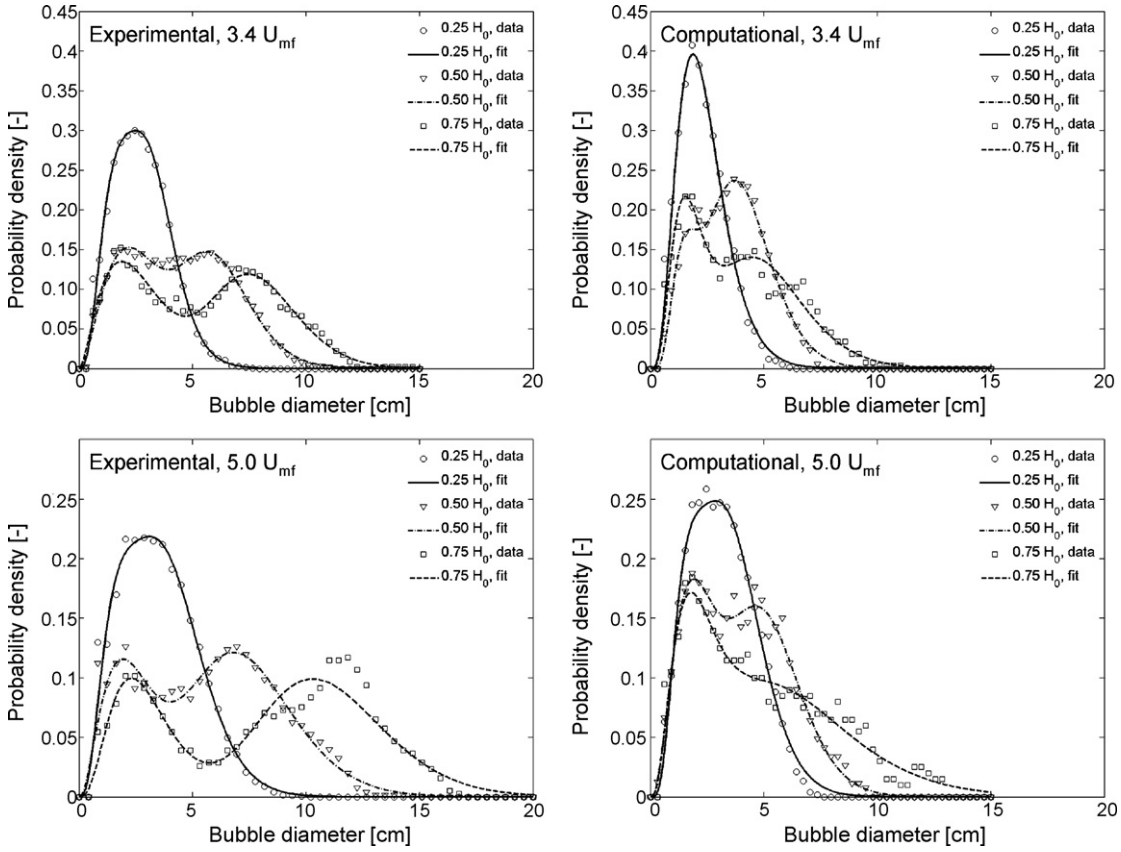

Fig. 10. Experimental and computational probability density distribution of bubble diameter at different distances from distributor and inlet gas velocities with relevant fitting curves ($u = 3.4$ and $5.0\,u_{mf}$).

exact form is not implemented in the Ansys CFX10.0 code. The code actually allows the granular temperature to be determined from the assumption of local equilibrium in the transport equation (i.e. Algebraic Equilibrium Model) which leads to the following simplified form of Eq. (21), adopted in this work:

$$\sigma_{si,j}\frac{\partial v_{si}}{\partial x_j} = \gamma_s \tag{22}$$

As far as the numerical aspects are concerned, CFD simulations were performed in a 2D fashion choosing a fixed time step interval $\Delta t = 10^{-3}$ s and a computational grid consisting of 5 mm square cells, with 288 cells along the vertical direction and 36 cells along the horizontal direction, thus resulting in a vertical extension of the domain equal to 1440 mm and an horizontal extension equal to 180 mm. Thus the width of the computational domain exactly coincides with that of the real lab-scale fluid-bed reactor experimentally investigated, while the height of the computational domain is in fact bigger than the real apparatus (i.e. 800 mm) in order to apply a fully developed flow condition at the top of the freeboard. Of course the initial condition for particle bed height at rest is identical to that of the experimental runs (i.e. 360 mm).

The lateral walls were modelled using the standard no-slip boundary condition. The upper section of the simulated geometry, or freeboard, was considered to be occupied only by gas. A simple pressure boundary condition was imposed at the top of freeboard (i.e. fully developed flow condition). A Dirichlet boundary condition was employed at the bottom of the bed to specify uniform vertical gas inlet velocity throughout the distributor. Symmetry planes were imposed on the front and rear faces of the simulated bed, in order to perform the simulation in a proper 2D fashion. Symmetry planes placed at the boundaries along the width direction of the computational domain causes all variables to be mathematically symmetric, with thus no diffusion across the boundary, except the component of velocity normal to the boundary which is anti-symmetric.

The initial conditions specify only the distribution of solid volume fraction within the bed of solids which was set equal to 0.65.

Typical running CPU times for this reference case were equal to about 3 h for 1 s of real time simulated with a fixed time step interval $\Delta t = 10^{-3}$ s on a Dell Dimension 8300 Personal Computer.

A finer grid and smaller time step intervals were also preliminary considered. In particular the cases reported in Table 1 were also tested.

The purpose of performing 3D simulations was that of assessing the suitability of adopting symmetry planes in 2D simulations, and the degree of accuracy that may be lost as a consequence of this choice. The symmetry plane adopted in 2D simulation describes the front and rear wall as free-slip walls with zero-valued fluxes through the plane itself, while in 3D simulations all walls are modelled using the standard no-slip boundary condition. In the fully 3D computational grid, six cells were placed along the width of the bed in order to develop physically correct profiles along bed width and ensure numerical stability of the simulation.

A preliminary comparison of the CFD results obtained from the reference case and the above first three cases allowed to state that a slight yet not significant improvement was achieved for the more CPU time consuming cases. In particular, all computational predictions appears not to have any systematic difference with reference to the comparison with experimental data, but only random differences due to the chaotic behaviour of such physical systems. Moreover, comparison of the reference case (Table 2) with the full 3D case (Case D in Table 2) indicated that the choice of 2D sim-

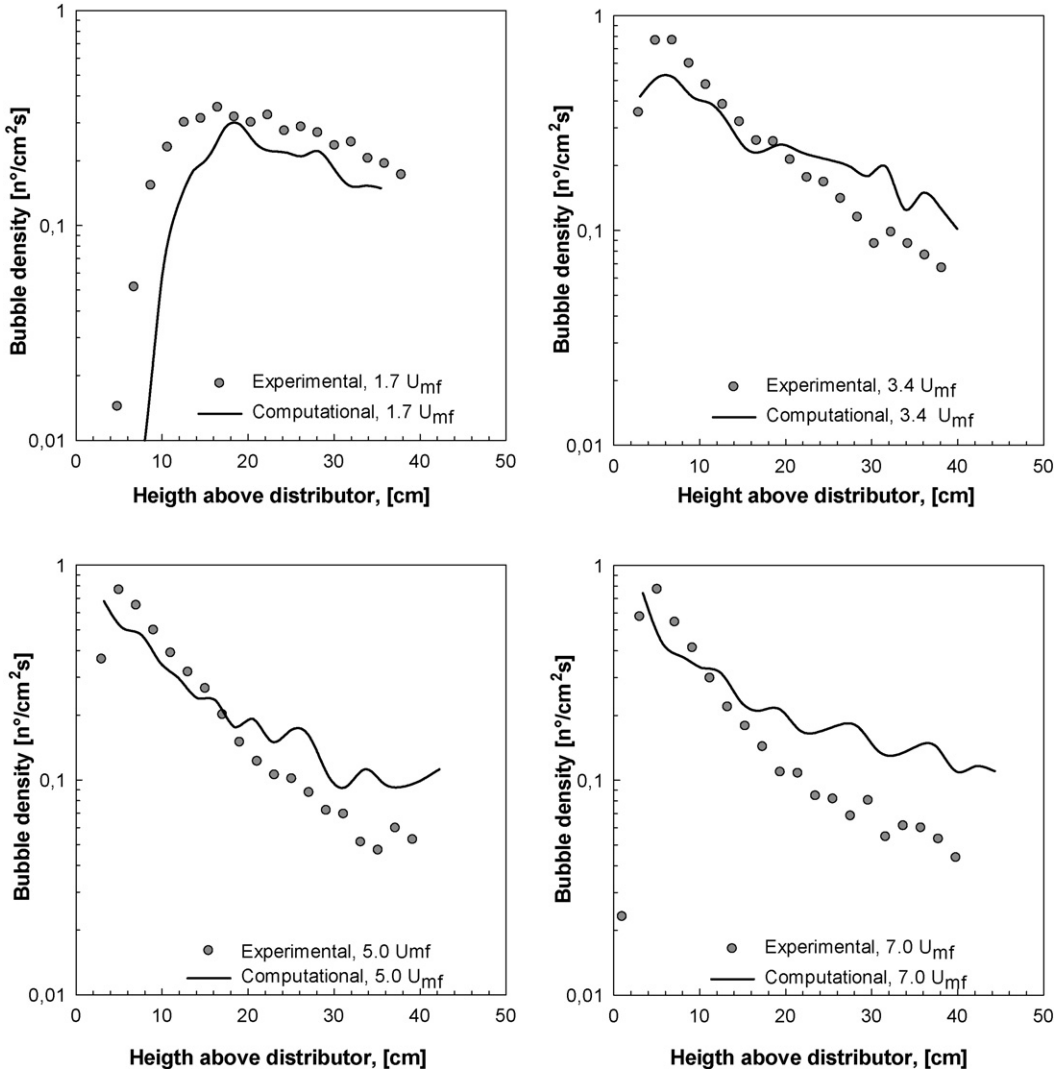

Fig. 11. Comparison of experimental (marks) and computational (lines) bubble density along bed height. (a) 1.7 u_{mf}, (b) 3.4 u_{mf}, (c) 5.0 u_{mf} and (d) 7.0 u_{mf}.

ulation gives rise to random differences in the simulated bubble properties less than 2%, practically not significant for engineering purposes.

On the above basis all results in the following have been obtained with by choosing the reference case conditions (Table 2) and the same gas velocities adopted for experiments (Table 1), in order to obtain fully comparable data.

5. Post-processing procedure via Digital Image Analysis Technique

The quantitative data on experimental and simulated bubble dynamics have been obtained by means of the Digital Image Analysis Technique (DIAT) presented in Part I of the present work [13], which the reader is referred to for full details.

This is based on bed images, appropriately obtained with backlighting in order to enhancing the contrast between the emulsion phase and the bubble phase. Bubbles in the bed could be detected because they create transparent areas in the flat cross-sectional plane of the bed, through which light, emitted at the back of the bed can pass through and reach the camera.

The problem of enhancing phase separation typical of experiments does not exist in simulation. As a matter of fact, by using the post-processing software available in the CFD code, it is possible to obtain the concentration field in the whole computational domain. The solid concentration field is then exported into the Matlab environment. The computational cells having solid volume fraction less than the conventional value of 0.15 [13], are considered as bubbles, while the other ones are considered as the emulsion phase.

The above-mentioned DIAT can be easily used for both experimental images and computational volume fraction maps, without any adjustment. The data obtained can be used to rebuild some important information about the bubble dynamics, such as

(i) Average bed height as function of time;
(ii) Bubbles hold-up as function of time;
(iii) Distribution of bubble equivalent diameters as function of bubble distance from the distributor;
(iv) Bubble aspect ratio, i.e. the ratio between the height and the width of the bubble;
(v) Average bubble number as function of the distance from the distributor.

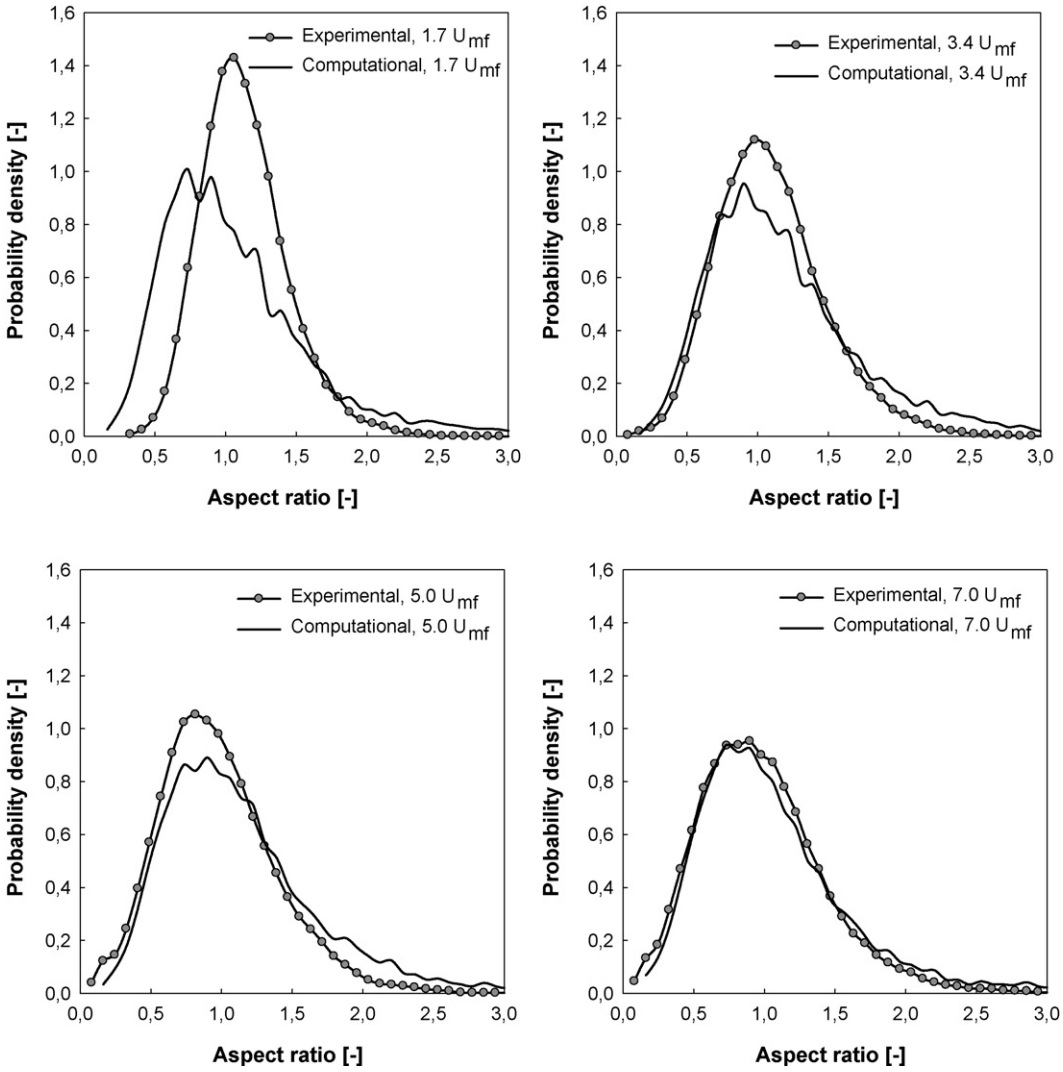

Fig. 12. Comparison of experimental (marks) and computational (lines) probability density function of bubbles aspect ratio. (a) 1.7 u_{mf}, (b) 3.4 u_{mf}, (c) 5.0 u_{mf} and (d) 7.0 u_{mf}.

As regards points (iii)–(v) the statistical analysis was performed by excluding all rising voids adherent to the lateral edges of the bed and those bursting at the top of the bed.

The rising velocity distribution was found by comparing bubble centroids positions in subsequent frames. Within the present work two kinds of different velocimetry approaches have been adopted: the Eulerian Velocimetry Technique (EVT) and the Lagrangian Velocimetry Technique (LVT), whose details have already been presented in [13].

The data processed by the use of the velocimetry techniques allow to rebuild fundamental information on bubble dynamics, such as

(i) Variation of bubble rise velocity with bubble diameter (EVT and LVT);
(ii) Distribution of velocity coefficient for Davidson type law (LVT);
(iii) Distribution of bubbles rise angles.

The direct comparison between these experimental and computational data on bubble dynamics allows coherent validation of the computer simulations of these bubbling fluidized beds.

6. Results and discussion

Computational results will be presented for all cases experimentally investigated and described in Table 1.

The first qualitative evaluation of simulation results can be easily performed by comparison of images reported in Fig. 2. In particular, Fig. 2a reports a typical sequence of volume fraction distribution maps, for the simulated case of glass ballotini d_p = 212–250 μm fluidized at $u = 1.7\ u_{mf}$. The sequence embraces all times from start-up to steady-state conditions (i.e. from 0.0 to 10.0 s), while only steady-state snapshots are given for the experimental case reported in Fig. 2b. The code appears to correctly simulate, at least in a qualitative way, the real behaviour of the system investigated. Bubble formation and growth along the bed appears to be correctly predicted by the code.

6.1. Global measurements via DIAT

6.1.1. Bed expansion

Fig. 3 reports the comparison between experimental and computational data for instantaneous bed height at $u = 3.4\ u_{mf}$: both experimental and computational data show the characteristic fluctuations of the free surface of the bed, due to the eruption of

bubbles. To quantify this behaviour, the mean value of bed expansion (i.e. the ratio between the instantaneous bed height and the settled bed height) and its standard deviation were computed for each case, the latter being a statistical measure of bed height instantaneous fluctuations.

In Fig. 4, the bed expansion data H/H_0 and the relative standard deviations are reported, on a semi-log chart, for all cases investigated as a function of the inlet gas reduced velocity, i.e. the ratio between the actual inlet gas velocity and u_{mf}.

Experimental data show that the mean expansion is characterized by a linear trend on the semi-logarithmic chart. It must be noted that the 212–250 μm particulate presents an expansion value of $1.16H/H_0$ at the lowest gas velocity of $1.7\,u_{mf}$, and increases up to a value of $1.47H/H_0$ when the inlet gas velocity reaches the value of $7.0\,u_{mf}$.

The analysis of standard deviations can be very helpful in assessing the amplitude of bed height fluctuations. In fact such fluctuations are mainly due to the bubble eruption phenomenon, i.e. bubbling intensity, which in turn depends upon bubble eruption frequency and bubble size. In this respect the standard deviations plotted in Fig. 4 are a qualitative measure of the bubbling intensity. The standard deviation value, as physically expected, increases with inlet gas reduced velocity for both particulate sizes.

The computational bed-height mean values are in acceptable agreement with experimental data on the whole. However, the code underestimates the expansion value at low inlet gas velocities. The underestimation appears to decrease at higher velocities, until at the highest velocity a slight overestimation is found. The linear trend observed on a semi-logarithmic chart is correctly predicted by the CFD simulation, but a slope slightly higher than that relevant to experimental data is observed.

After all, the comparison between computational and experimental data shows the capability of the code to adequately predict the variation of both mean values of bed expansion and relevant standard deviation with fluidization velocity.

6.1.2. Overall bubble hold-up

In Fig. 5, the comparison between experimental and computational data on instantaneous bubble hold-up is reported for the case of 212–250 μm glass ballotini and inlet gas velocity $u = 3.4\,u_{mf}$: the data are computed by dividing the sum of bubble projected areas by the total projected area occupied by the bed. Both experimental and computational data show significant fluctuations due to the dynamic of formation and eruption of the bubbles. It must be observed that the bed expansion dynamic plotted in Fig. 3 and the bubble hold-up dynamic in Fig. 5 are rather different. Bed expansion depends on both the extent of the bubble phase and the expansion of the emulsion phase, bubble hold-up measures just bubbles overall content.

The bubble hold-up mean value and its standard deviation is computed for each case and reported in Fig. 6, as function of the ratio u/u_{mf} on a semi-log chart. A linear trend is found, similar to that observed in the analysis of bed expansion. The code generally underestimates the mean bubble hold-up, especially at higher inlet gas velocities. The general underestimation of bubble hold-up values could be due to an underestimation of bubble diameters and/or bubble density, although the qualitative trend is correctly predicted by numerical simulations. Conversely, the bubble hold-up standard deviations predicted by simulation are in fair agreement with experimental ones.

In particular, the comparison between Figs. 4 and 6 reveals that the CFD code capability to predict even such simple global behaviour is not entirely satisfactory: at the lowest gas velocities, both bed expansion and bubble hold up are underestimated. It is worth noting that the important underestimation of bed expansion is only partially due to the slight underestimation of bubble hold up, and also related to the incorrect prediction of void fraction of the emulsion phase, both in its bulk and in the transition region between the emulsion phase and the bubble phase. Conversely, at higher velocities the code overestimates the bed expansion even if the bubble hold up is underestimated. This can be principally attributed to problems in the simulation of the transition region near the bubble, a region that generally appears more widespread with respect to experimental data.

6.1.3. Local bubble hold-up distribution

Fig. 7 reports the comparisons between the predicted and experimental local bubble hold-up distribution maps for all investigated cases.

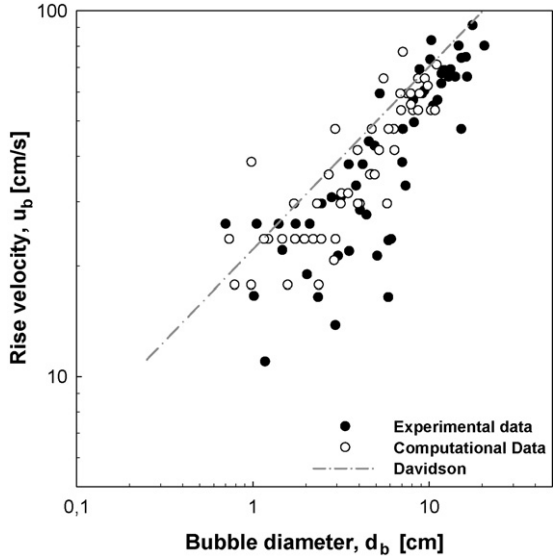

Fig. 13. Experimental and computational distribution of bubble rise velocities as function of bubble equivalent diameter for all investigated cases computed by the means of EVT compared with the Davidson and Harrison [52] correlation.

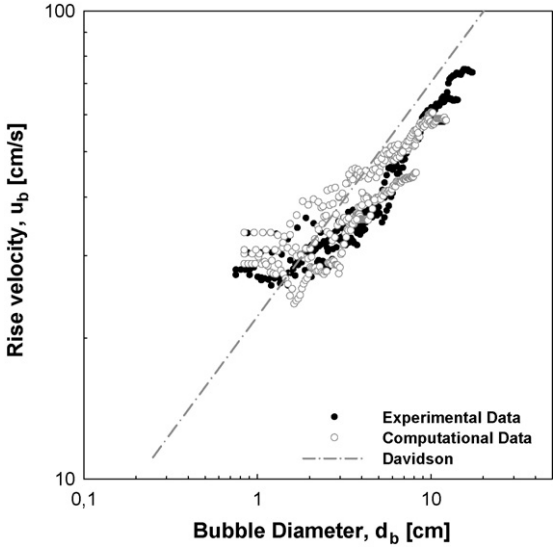

Fig. 14. Comparison of experimental and computational distribution of bubble rise velocities as function of bubble equivalent diameter for all investigated cases computed by the means of LVT.

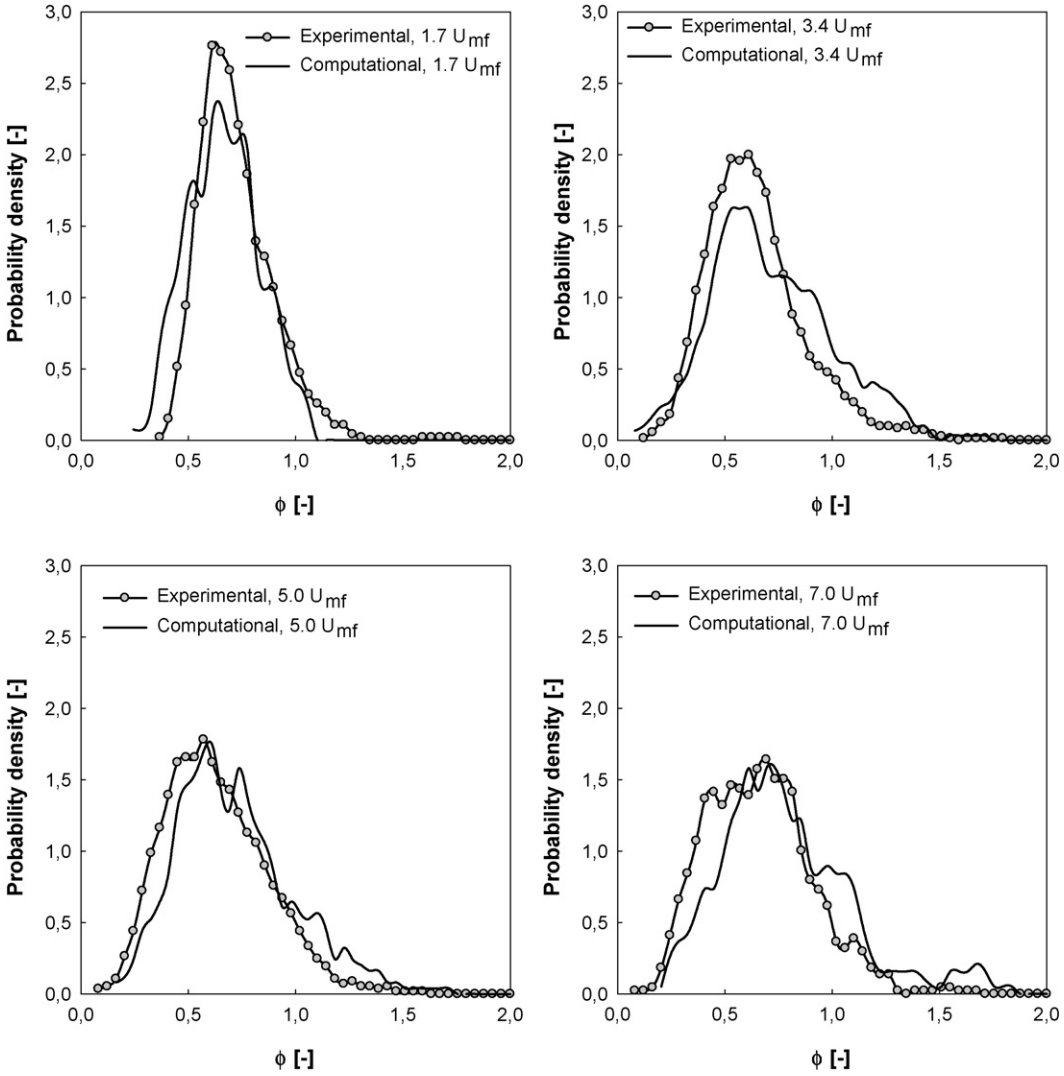

Fig. 15. Comparison between experimental and computational probability density function of Davidson's coefficient.

The analysis of experimental time-averaged bubble phase hold-up allows the visual observation of preferential bubble paths along the bed, with a typical reverse-Y-shaped pattern starting near the bottom of the bed and developing in the upper regions of the bed. The reverse-Y-shaped pattern is due to the coalescence-driven bubble dynamics prevailing after bubble nucleation in the proximity of the distributor in the intermediate region of the bed. In particular, the analysis of 212–250 μm particulate maps allows the observation and quantification of systematic trends in bubbles path characteristics, with the only exception of $1.7\,u_{mf}$ map, in which the filtering of smaller bubbles does not allow observation in the lower region of the bed. At low inlet gas velocity, bubbles appear to almost uniformly rise through the bed. Increasing inlet gas velocity, the tendency for bubbles to follow the reverse-Y path in the lower region of the bed increases, while the void distribution in the proximity of the bed surface appear to be less sharp, due to more intense eruption of bubbles.

It is worth noting that the straight-vertical path in the upper sections of the bed appear to be straighter and thinner with increasing gas velocity, as a consequence of the formation of greater bubbles, rising up through the bed undisturbed because of a less significant presence of coalescence phenomena.

As far as the numerical predictions are concerned, CFD results fail to accurately predict the experimental measured values of bubble local hold up. Although an increasing trend of hold-up values with inlet gas velocity is found, the shape of the distribution and its relevant numerical values are not fully correctly predicted for the cases here investigated. For the case of 212–250 μm particulate, the bubble hold up distribution maps computed by the simulation show bubbles to be randomly distributed along bed width, while the experiments are characterized by a preferential path.

On the whole, although the code predicts the onset of bubbling, specific features such as initial formation of slugs in upper regions of the bed are not correctly predicted for all cases simulated at high inlet gas velocity. The simulated bubbling behaviour appears to be more similar to normal bubbling with greater bubbles, rather than being capable of correctly predicting the onset of slugging.

6.2. Bubbles properties measurements via DIAT

6.2.1. Bubble size evolution

In Fig. 8, the experimental and computational distributions of bubble equivalent diameters are reported as function of bubble distance from distributor. The full set of data is presented in raw

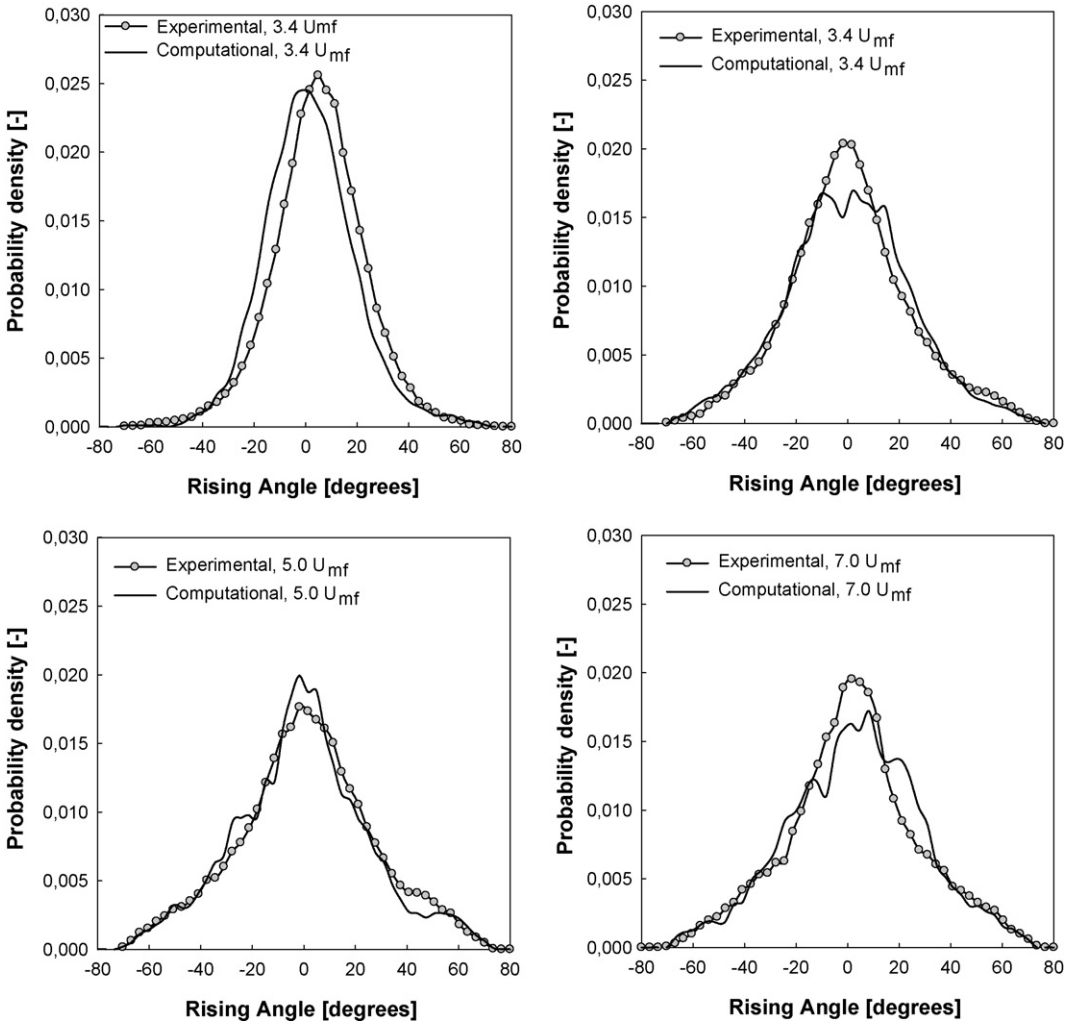

Fig. 16. Comparison between experimental and computational probability density function of bubble rising angle.

cloudy form, in order to highlight the complex bubble behaviour along bed height. The adoption of an average curve with indication of its variance would not account for the richness of the raw data. Conversely, the cloudy data presented allow the visualization of the small bubbles that are inside the bed even at the highest elevations, while an average curve, even if with variance, could not show such characteristic and complexity.

On the whole the experimental data show a characteristic increase in bubble diameter, with an upper envelope of data approximately following a power law, in accordance with the analysis by Darton et al. [35]. However, the presence of a wide distribution of bubble sizes is evident at all elevations of the bed, as a result of the splitting and/or nucleation phenomena.

At increasing gas velocities, the increase in bubble diameter is more pronounced, as physically expected. Moreover, the presence of small bubbles in upper regions of the bed appear to be less pronounced with increasing velocity, due to the onset of slugs in such regions.

As far as the numerical predictions are concerned, the computational results reported are in good agreement with experimental data only at lower gas velocity, with some limited level of underestimation. In all other cases the CFD results show a positive agreement only in the lower regions of the bed, while at higher elevations bubble diameters are under-predicted, up to 30% in the worst case.

6.2.2. Bubble size distribution (BSD)

In Fig. 9, the experimental and computational distributions of bubble equivalent size distribution are reported. The experimental distributions show a characteristic positive skewness of the distributions at all inlet gas velocities, in accordance with relevant literature data [46–51]. It is worth noting that at lower inlet gas velocities the right-hand tail of the distribution has a concave-up shape, as a result of the predominant coalescence phenomenon, which causes bubbles to increase their diameter by coalescence with similar bubbles. Conversely at higher inlet gas velocities an almost linear decay is observed, due to the onset of slugs, which essentially grow by including along their rising path all other bubbles.

Computational predictions of bubble size distributions show a general acceptable agreement regarding the shape of distribution in all cases so far investigated, but the CFD results fail to predict the presence of an almost linear right-hand tail of the distribution for the cases of high inlet gas velocities. This confirms the inability of the model here adopted to correctly simulate the onset of slug flows. Moreover, statistical distribution presents shorter right-hand tails. Such apparently small difference has a large influence on the overall prediction of the bubble hold-up and bubble size evolution, since the right-hand tail of the distribution is relative to large bubbles, which are responsible for carrying considerable amounts of gas volumes along the bed.

The bubble size distribution in the whole bed assumed the characteristic shape of a positively skewed monomodal distribution, as expected from the relevant already cited literature. Conversely, the analysis of all investigated bubble size distributions computed in regions at different elevations above the distributor (i.e. $0.25H_0$, $0.50H_0$, $0.75H_0$ for the case of particles fluidized at 3.4 and $5.0\,u_{mf}$) shows a characteristic bimodality of BSD, that can be somewhat inferred from Fig. 8, and is also self-evident in Fig. 10.

The different shapes of local BSD at different elevations can be ascribed to the coalescence and break-up phenomena occurring in the fluidized bed. In fact, at each elevation analyzed, with the exception of the measurements taken at $0.25H_0$, it is possible to find a fraction of bubbles having considerably smaller size than that expected at that particular elevation, whose genesis is related to nucleation and break-up phenomena occurring at that elevation. Conversely the complementary fraction of bubbles having the expected size for that elevation naturally originates from coalescence and growth of bubbles from inferior regions of the bed.

This mechanism is able to describe the bimodal pattern of BSD in fluidized beds: the primary peak (i.e. smaller bubble sizes) is due to local nucleation and splitting phenomena, and thus its mean and mode value does not change with elevation above the distributor. Conversely, the secondary peak (i.e. larger bubble sizes) will increase its mean and mode value with the elevation, as physically expected because of the above-mentioned coalescence phenomena. The bimodal pattern of local BSD is a substantially new finding with respect of the previous works regarding fluidized beds BSD. It is worth noting that the code is able of reproducing such behaviour, even if only in a qualitative manner, as can be seen in Fig. 10. In fact a sort of bimodality appears in both computational cases presented, but in all cases narrower distributions are found, whose shapes appear quite similar to those obtained by Patil et al. [22]. Moreover, the use of local BSD helps to highlight the discrepancy in the prediction of large bubble formation already discussed in this paragraph.

6.2.3. Bubble density

In Fig. 11, the experimental and computational bubble density profiles along the bed height is reported. It must be pointed out that a linear decay of bubble density on a logarithmic chart would characterize a constant bubble coalescence rate, while a constant value of bubble density would be typical of fully developed slug flow.

The experimental data reported in Fig. 11 show an almost similar behaviour at all inlet gas velocities, except for the case of the lowest velocity (i.e. $u = 1.7\,u_{mf}$). In this last case the data show an increasing trend near the distributor, where the bubbles are characterized by small diameters. This occurrence is likely to generate a sensitivity problem for the technique here adopted. In fact, the bubble filtering procedure adopted to eliminate false bubbles, extensively discussed in Part I of this work, cuts most of the smallest bubbles, thus invalidating the bubble count in this region of the bed. The experiments with higher inlet gas velocities, thanks to the generation of larger bubbles do not have such problem, showing an increasing constant decay rate with increasing inlet gas velocity. However, the presence of a region near the freeboard with lower values of the decay rate, due to the local transition to slugging regime, is also correctly found.

As far as numerical simulations are concerned, predictions show in all cases a linear trend similar to that of experiments, although they fail in quantitatively predicting the decay rates. In fact the simulation seem to predict a linear decay trend whose slope does not change appreciably with inlet gas velocity. These facts confirm the difficulty of the code in predicting the flow regime transition between the bubbling and slugging regimes.

6.2.4. Bubble aspect ratio

In Fig. 12, the experimental and computational distributions of bubble aspect ratio are reported. In the present work the aspect ratio is actually defined as the ratio between the bubble maximum horizontal extension and its maximum vertical extension. For more detailed considerations on this parameter the reader is referred to Part I of the present work [13].

The analysis of experimental distributions show an increase of the skewness of the distribution with increasing inlet gas velocity. This is likely due to the increase of vertically oblong bubbles, as physically expected. This finding is confirmed by a slight decrease in the distribution modes.

On the other hand the distribution obtained by numerical predictions appear not to change significantly with increasing inlet gas velocity, for all cases presently investigated. This evidence confirms once again that numerical simulations are still not satisfactory to predict the bubble shape, and in particular the transition between the bubbling and slugging regimes.

6.3. Bubbles velocimetry

6.3.1. Bubble velocity distribution via EVT and LVT

Fig. 13 reports the computational and experimental averaged bubble rise velocity distribution obtained by EVT, while Fig. 14 reports both the experimental and computational averaged bubble rise velocity distributions obtained by LVT as functions of the bubble equivalent diameter. In both figures, no distinction is made between the different investigated cases, since a preliminary investigation confirmed that bubble velocity depends only on bubble diameter. On these grounds, data in Figs. 13 and 14 are only divided in computational and experimental data series.

A comparison with the power law by Davidson and Harrison [52], who proposed

$$u_b = \phi(g d_b)^{0.5} \tag{23}$$

with a value for the velocity coefficient $\phi \approx 0.71$, show in both figures that the experimental rise velocities measured by EVT appear to be somewhat overestimated by Davidson's correlation, especially in the range of smaller diameters.

CFD simulation results were reported in Fig. 13 gave rise to loss of sensitivity (generating identical velocity values for different bubble diameters), due to the combination of image resolution and frame rate used for computational data measurement. The same problem, although at a very small extent, also appears in the experimental data shown in the same figure.

Such problems can be eventually solved, in both simulations and experiments, by an accurate choice of frame rate and image definition. An increase in reliability of the procedure can be obtained by substituting the commercial camera used in this work with a medium-high fps camera (50–200 fps) having sufficiently high resolution (at least 1024×760 pixels).

As far as the LVT is concerned, the relevant averaged data are reported in Fig. 14, and compared with relevant literature correlation prediction. The power law proposed by Davidson appear to acceptably predict the general trend in increase of bubble rise velocity with increasing bubble diameter, even if a slight overestimation is still evident.

Computational results obtained by LVT are also reported in Fig. 14. The data scattering, due to the chaotic nature of the investigated systems, is well simulated and in sound agreement with experiments.

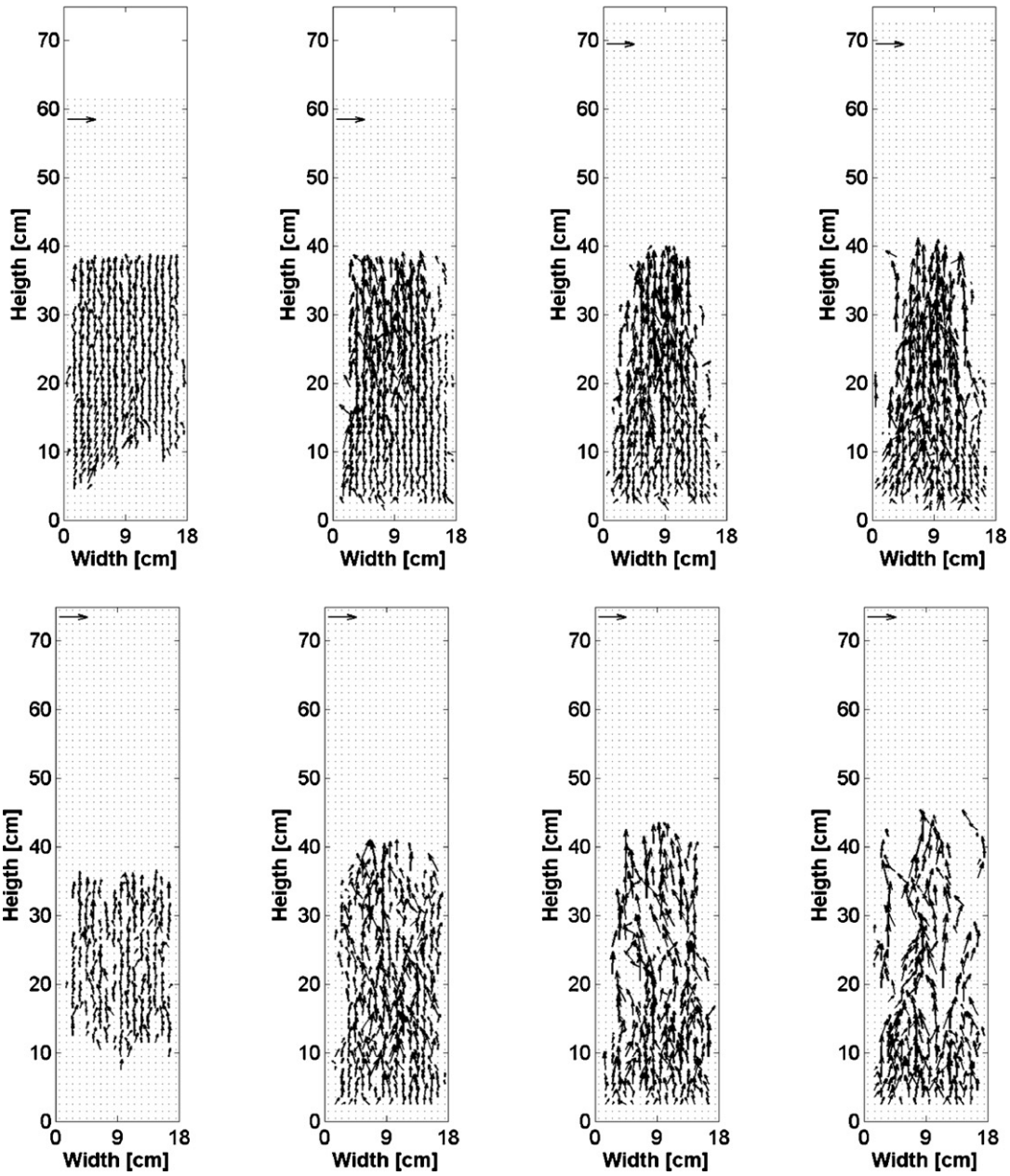

Fig. 17. Experimental (superior row), and computational (inferior row) bubble vector plots, from left to right 1.7 u_{mf}, 3.4 u_{mf}, 5.0 u_{mf} and 7.0 u_{mf}. *Reference vector* = 100 cm s^{-1}.

6.3.2. Bubble velocity coefficient distribution via LVT

Comparisons between the experimental and computational distributions of the bubble velocity coefficient (i.e. Eq. (23)) are reported in Fig. 15. The coefficients are computed by using the LVT bubble tracking data suitably processed by fitting the bubble vertical trajectories during their whole life (from nucleation or splitting to eruption or coalescence).

The analysis of experimental data shows a complex behaviour with increasing inlet gas velocity. The measured skewed distributions appear to be larger with increasing gas velocity, with significant scatter observed. On the contrary, the modes of the distribution appear to be negligibly influenced by the gas velocity.

The comparison of simulation results with experimental data highlights a substantial agreement for the cases investigated, with errors likely to be due to experimental data scattering rather than incorrectness of the predictions.

The values of the coefficients appear to be similar to that proposed by Darton ($\phi = 0.71$), while the correlation developed by Shen et al. [53], gives rise to a value of the velocity coefficient in the range [0.8–1], quite different from the mean values found in this work.

6.3.3. Bubble rise angle distribution via LVT

Fig. 16 reports the probability distribution of rising angles for each investigated case. In each graph the experimental and the computational data are compared.

It is worth noting that this parameter exhibits an almost symmetrical Gaussian distribution at the lowest velocities, while at higher velocities more complex symmetrical distributions are found. In particular the distribution shape here found approximately follows a Gaussian distribution near the mode value. It should be observed that both tails are almost linear, and quite different from the expected Gaussian distribution. This shape can be interpreted as the sum of two different zero-mean random devia-

tions from the natural vertical path of the bubble. The first is due to the random lateral motion of the bubble in the presence of other bubbles perturbating the general flow field in the fluidized bed, and give rise to the low angle symmetrical deviations. The second is due to the capture motion of small bubbles when coalescence occurs. This latter motion is strongly directional for each single bubble, however resulting in a symmetrical distribution because of the geometrical symmetry of the entire system.

It is worth noting that the comparison between the experimental and computational distributions show a very good agreement, thus confirming the coalescence capture motion prediction capability of the code at all gas velocities here investigated.

6.3.4. Overall bubble velocity fields

Finally, in Fig. 17 the experimental and computational bubbles vector plots are reported for all investigated cases. The plots are obtained by suitable time averaging of instantaneous bubble velocity maps.

In accordance to the previous discussions, bubble trajectories would be slightly oriented towards the centre of the bed in the lower part of the bed and then vertically directed in the upper section of the bed. Moreover, the velocity field plots confirm the evidence for the local bubble hold-up maps shown in Fig. 7. These latter allow the visualization of preferential bubble paths along the bed height, whereas the former associates the relevant bubble average velocities to preferential paths.

Interestingly vector plots from experimental data show bubble averaged trajectories oriented towards the centre of the bed in the lower part of the bed, where most of the coalescence phenomena takes place, and from there they are subsequently directed vertically in the upper section. It should be moreover observed that such behaviour is increasingly more definite at higher gas velocities.

Simulation results are also in sound agreement with such experimentally observed behaviour although a larger data scattering is somewhat evident.

7. Conclusions

The Digital Image Analysis Technique presented in Part I of this work [13] has been successfully applied not only to the data on gas–solid fluidization obtained by purposely performed experiments, but also for the first time to data from numerical simulations performed by a commercial CFD code.

A first comment is to be made on the application of the present methodology to both sets of experimental data and computational results. In particular the use of the very same DIAT method to both sets of data allows for a fully consistent quantitative comparison of the very same physical quantities, overcoming the well known problem of comparison sensitivity to the differences in the experimental measurement techniques and numerical post-processing computations.

With regards to the analysis of the experimental data a first major outcome has been the production of an extended set of detailed quantitative information on bubble dynamics. Moreover, thanks to the use of DIAT some novel results have been obtained. Firstly the finding of a bimodality for the local BSD at all elevations highlighted the richness and complexity of the bubbling dynamics, which includes bubble break-up and coalescence phenomena. Secondly the velocity coefficient distributions appeared to be slightly smaller, on overall, with respect to those obtained by previous works for 2D bubbling beds.

As far as the CFD predictions are concerned, many features of the bubbles were compared with the aim of thoroughly validating the CFD results. These features comprise average bed height, bubbles hold-up, distribution of bubble equivalent diameters, bubble aspect ratio, bubble number, bubble rise velocity and velocity coefficient, bubbles rise angles and their dependence on various parameters. As regards the global indicators, they in general show a good agreement between experiments and simulations. However, in all cases here tested a general low sensitivity of the simulations was observed in order to correctly predict the change of the bubbling behaviour with increasing inlet gas velocity as well as with elevation above the distributor.

On overall thanks to the extensive validation here performed by means of DIAT, the fully predictive CFD model here tested appears to have the potential to be useful for design and development of bubbling fluidized beds, although further development of the currently implemented CFD models is required.

Acknowledgements

In loving memory of Luca Cammarata whose promising research efforts into the field of fluidization were so prematurely forced to end. This work was carried out within the framework of the PRIN 2005 research program “Study of fluidized beds stabilized by means of electric or magnetic fields” funded by the Italian Ministry of University.

References

[1] F. Johnsson, S. Andersson, B. Leckner, Expansion of a freely bubbling fluidized bed, Powder Technol. 68 (1991) 117–123.
[2] P.N. Rowe, D.J. Everett, Fluidised bed bubbles viewed by X-rays. Part I. Experimental details and the interaction of bubbles with solid surfaces, Trans. Inst. Chem. Eng. 50 (1972) 42–48.
[3] P.N. Rowe, D.J. Everett, Fluidised bed bubbles viewed by X-rays. Part II. The transition from two to three dimensions of undisturbed bubbles, Trans. Inst. Chem. Eng. 50 (1972) 49–54.
[4] P.N. Rowe, D.J. Everett, Fluidised bed bubbles viewed by X-rays. Part III. Bubble size and number when unrestrained three dimensional growth occurs, Trans. Inst. Chem. Eng. 50 (1972) 55–60.
[5] P.K. Agarwal, Bubble characteristics in gas fluidized beds, Chem. Eng. Res. Des. 39 (1985) 323–337.
[6] J.S. Sung, J.M. Burgess, A laser based method for bubble parameter measurement in two dimensional-fluidized beds, Powder Technol. 49 (1987) 165–175.
[7] L.R. Glicksman, W.K. Lord, M. Sakagami, Bubble properties in large particle fluidized beds, Chem. Eng. Sci. 42 (1987) 479–491.
[8] C.M. Atkinson, N.N. Clark, Gas sampling from fluidized beds: a novel probe system, Powder Technol. 54 (1988) 59–70.
[9] K.S. Lim, P.K. Agarwal, Conversion of pierced lengths measured at a probe to bubble size measures: an assessment of the geometrical probability approach and bubble shape models, Powder Technol. 63 (1990) 205–219.
[10] J.S. Halow, G.E. Fasching, P. Nicoletti, J.L. Spenik, Observation of a fluidized bed using capacitance imaging, Chem. Eng. Sci. 48 (1993) 643–659.
[11] D. Gera, M. Gautam, Bubble rise velocity in two-dimensional fluidized beds, Powder Technol. 84 (1995) 283–285.
[12] A.S. Hull, Z.M. Chen, J.W. Fritz, P.K. Agarwal, Influence of horizontal tube banks on the behaviour of bubbling fluidised beds. 1. Bubble hydrodynamics, Powder Technol. 103 (1999) 230–242.
[13] A. Busciglio, G. Vella, G. Micale, L. Rizzuti, Analysis of the bubbling behaviour of 2D gas fluidized beds. Part I. Digital Image Analysis Technique, Chem. Eng. J. 140 (2008) 398–413.
[14] M.A. Gilbertson, J.G. Yates, The motion of particles near a bubble in a gas-fluidized bed, J. Fluid Mech. 323 (1996) 377–385.
[15] C.C. Pain, S. Mansoorzadeh, C.R.E. de Oliveira, A study of bubbling and slugging fluidised bed s using the two-fluid granular temperature model, Int. J. Multiphas. Flow 27 (2001) 527–551.
[16] S. Chapman, T.G. Cowling, The Mathematical Theory of Non-uniform Gases, 3rd ed., Cambridge University Press, Cambridge, UK, 1970.
[17] J.L. Sinclair, R. Jackson, Gas–particle flow in a vertical pipe with particle–particle interactions, AIChE J. 35 (1989) 1473–1486.
[18] J. Ding, D. Gidaspow, A bubbling fluidization model using kinetic theory of granular flow, AIChE J. 36 (1990) 523–538.
[19] C.M. Hrenya, J.L. Sinclair, Effects of particle-phase turbulence in gas–solid flows, AIChE J. 43 (1997) 853–869.
[20] M.J.V. Goldschmidt, J.A.M. Kuipers, W.P.M. Van Swaaij, Hydrodynamic modelling of dense gas-fluidised beds using kinetic theory of granular flow: effect of coefficient of restitution on bed dynamics., Chem. Eng. Sci. 56 (2001) 571–578.
[21] S.J. Gelderbloom, D. Gidaspow, R.W. Lyczkowski, CFD simulations of bubbling/collapsing fluidized beds for three Geldart groups, AIChE J. 49 (2003) 844–858.

[22] D.J. Patil, M. Van Sint Annaland, J.A.M. Kuipers, Critical comparison of hydrodynamic models for gas–solid fluidized beds.Part II. Freely bubbling gas–solid fluidized beds, Chem. Eng. Sci. 60 (2005) 73–84.
[23] R. Clift, J.R. Grace, M.E. Weber, Bubbles, Drops and Particles, Academic Press, London, UK, 1978.
[24] R.B. Bird, W.E. Stewart, E.N. Lightfoot, Transport Phenomena, 2nd ed., Wiley, New York, 2002.
[25] C.Y. Wen, Y.H. Yu, Mechanics of fluidization, Chem. Eng. Prog. Symp. Ser. 62 (1966) 100–111.
[26] M. Syamlal, T.J. O'Brien, Computer simulation of bubbles in a fluidized bed, AIChE Symp. Ser. 85 (1989) 22–31.
[27] M. Syamlal, W. Rogers, T.J. O'Brien, Mfix Documentation Theory Guide, Technical note DOE/METC-94/1004, U.S. Department of Energy, Office of fossil energy, 1993.
[28] D. Gidaspow, Multiphase Flow and Fluidization, Academic Press, San Diego, 1994.
[29] L. Mazzei, P. Lettieri, A drag force closure for uniformly dispersed fluidized suspensions, Chem. Eng. Sci. 62 (2007) 6129–6142.
[30] J.R. Grace, F. Taghipour, Verification and validation of CFD models and dynamic similarity for fluidized beds, Powder Technol. 139 (2004) 99–110.
[31] D. Gidaspow, B. Ettehadieh, Fluidization in two-dimensional beds with a jet hydrodynamic modelling, Ind. Eng. Chem. Fundam. 22 (1983) 193–201.
[32] J.X. Bouillard, R.W. Lyczkowski, D. Gidaspow, Porosity distributions in a fluidized bed with an immersed obstacle, AIChE J. 35 (1989) 908–922.
[33] J.A.M. Kuipers, K.J. Van Duin, F.P.H. Van Beckum, W.P.M. Van Swaaij, Computer simulation of the hydrodynamics of a two dimensional gas-fluidized bed, Comput. Chem. Eng. 17 (2003) 839–858.
[34] B.G.M. Van Wachem, J.C. Schouten, R. Krishna, C.M. van den Bleek, Eulerian simulations of bubbling behaviour in gas–solid fluidised beds, Comput. Chem. Eng. 22 (Suppl. 1) (1998) S299–S306.
[35] R.C. Darton, R.D. La Nauze, J.F. Davidson, D. Harrison, Bubble growth due to coalescence in fluidised beds, Trans. IChemE 55 (1977) 274–280.
[36] E. Peirano, V. Delloume, B. Leckner, Two or three-dimensional simulations of turbulent gas–solid flows applied to fluidization, Chem. Eng. Sci. 56 (2001) 4787–4799.
[37] M. Ishii, Thermo-fluid dynamic theory of multi-phase flow, Collection de la Direction des Etudes et Researches d'Electricité de France, Eyrolles, Paris, France, 1975.
[38] D.J. Patil, M. van Sint Annaland, J.A.M. Kuipers, Critical comparison of hydrodynamic models for gas–solid fluidized beds. Part I. Bubbling gas–solid fluidized beds operated with a jet, Chem. Eng. Sci. 60 (2005) 57–72.
[39] Z. Chen, L.G. Gibilaro, P.U. Foscolo, Two-dimensional voidage waves in fluidized beds, Ind. Eng. Chem. Res. 38 (1999) 610–620.
[40] L.G. Gibilaro, Fluidization-Dynamics, Butterworth–Heinemann, Oxford, 2001.
[41] P. Lettieri, S. Brandani, J.G. Yates, D. Newton, A generalization of the Foscolo and Gibilaro particle-bed model to predict the fluid bed stability of some fresh FCC catalysts at elevated temperatures, Chem. Eng. Sci. 56 (2001) 5401–5412.
[42] S. Brandani, K. Zhang, A new model for the prediction of the behaviour of fluidized beds, Powder Technol. 163 (2006) 80–87.
[43] O. Owoyemi, P. Lettieri, R. Plac, Experimental validation of Eulerian–Eulerian simulations of rutile industrial powders, Ind. Eng. Chem. Res. 44 (2005) 9996–10004.
[44] P. Lettieri, R. Di Felice, P. Pacciani, P. Owoyemi, CFD modelling of liquid fluidized beds in slugging mode, Powder Technol. 167 (2006) 94–103.
[45] L. Mazzei, P. Lettieri, T. Elson, D. Colman, A revised mono-dimensional particle bed model for fluidized beds, Chem. Eng. Sci. 61 (2006) 1958–1972.
[46] D.T. Argyriou, H.L. List, R. Shinnar, Bubble growth by coalescence in gas fluidized beds, AIChE J. 17 (1971) 122–130.
[47] S. Morooka, K. Tajima, T. Miyauchi, Behaviour of gas bubble in fluid beds, Int. Chem. Eng. 12 (1972) 168–174.
[48] J. Werter, Bubbles in gas fluidized beds: part I, Trans. Inst. Chem. Eng. 52 (1974) 149–159.
[49] P.N. Rowe, C. Yacono, The distribution of bubble size in gas fluidized beds, Trans. Inst. Chem. Eng. 53 (1975) 59–60.
[50] W. Liu, N.N. Clark, Relationships between distributions of chord lengths and distributions of bubble sizes including their statistical parameters, Int. J. Multiphas. Flow 21 (1995) 1073–1089.
[51] C.E.J. Van Lare, H.W. Piepers, J.N. Schoonderbeek, D. Thoenes, Investigation on bubble characteristics in a gas fluidized bed, Chem. Eng. Sci. 52 (1997) 829–841.
[52] J.F. Davidson, D. Harrison, Fluidised Particles, Cambridge University Press, 1963.
[53] L. Shen, F. Johnsson, B. Leckner, Digital image analysis of hydrodynamics two-dimensional bubbling fluidized beds, Chem. Eng. Sci. 59 (2004) 2607–2617.